SANTA CATARINA STATE UNIVERSITY – UDESC
COLLEGE OF TECHNOLOGICAL SCIENCE – CCT
MASTER IN MECHANICAL ENGINEERING – PPGEM

DISSERTAÇÃO DE MESTRADO

METHODOLOGY TO EVALUATE THE FATIGUE LIFE OF SINTERTED CONNECTING ROD APPLIED TO RECIPROCATING COMPRESSOR

FÁBIO MEDEIROS DE LIMA

JOINVILLE, 2018

FÁBIO MEDEIROS DE LIMA

METHODOLOGY TO EVALUATE THE FATIGUE LIFE OF SINTERED CONNECTING ROD APPLIED TO RECIPROCATING COMPRESSOR

Master thesis submitted to the Mechanical Engineering Department at the College of Technological Science of Santa Catarina State University in fulfillment of the partial requirement for the Master's degree in Mechanical Engineering.

Advisor: Dr. Renato Barbieri

JOINVILLE

2018

Medeiros de Lima, Fábio
Methodology to evaluate the fatigue life of sintered connecting rod applied to reciprocating compressor / Fábio Medeiros de Lima. - Joinville , 2018.
80 p.

Orientador: Renato Barbieri
Dissertação (Mestrado) - Universidade do Estado de Santa Catarina, Centro de Ciências Tecnológicas, Programa de Pós-Graduação em Engenharia Mecânica, Joinville, 2018.

1. Reciprocating compressor. 2. Connecting rod. 3. Fatigue. I. Barbieri, Renato. II. Universidade do Estado de Santa Catarina. Programa de Pós-Graduação. III. Título.

METHODOLOGY TO EVALUATE THE FATIGUE LIFE OF SINTERED CONNECTING ROD APPLIED TO RECIPROCATING COMPRESSOR

por

Fábio Medeiros de Lima

Esta dissertação foi julgada adequada para obtenção do título de

MESTRE EM ENGENHARIA MECÂNICA

Área de concentração em "Modelagem e Simulação Numérica"
e aprovada em sua forma final pelo

CURSO DE MESTRADO ACADÊMICO EM ENGENHARIA MECÂNICA
DO CENTRO DE CIÊNCIAS TECNOLÓGICAS DA
UNIVERSIDADE DO ESTADO DE SANTA CATARINA.

Banca Examinadora:

Prof. Dr. Renato Barbieri
CCT/UDESC (Orientador/Presidente)

Prof. Dr. César Edil da Costa
CCT/UDESC

Dr. Rinaldo Puff
Whirlpool/Embraco

Joinville,SC, 28 de fevereiro de 2018.

RESUMO

O projeto de mecanismo de compressor alternativo é altamente dependente da definição de sua biela. Este componente, geralmente sinterizado, é desenvolvido para converter o movimento rotacional do motor elétrico em movimento linear do pistão, absorver os desvios geométricos dos componentes do mecanismo e suportar as cargas de operação do envelope de aplicação.

Logo, o comportamento a fadiga desse importante componente deve ser avaliado através de simulações numéricas, testes experimentais em bancada e confiabilidade em campo para prever possíveis modos de falha causados por diferentes condições de contorno de operação, caracterizadas pela combinação de flexão e compressão.

O presente trabalho explora as propriedades mecânicas de biela sinterizada em combinação estática e dinâmica de cargas de tração e compressão. Duas curvas S-N com níveis de tensão média compressiva e nula são associadas para gerar um critério de fadiga e calcular o coeficiente de segurança da biela, quando operando dentro do envelope de aplicação do compressor.

Palavras chave: Compressor Alternativo, Biela, Fadiga.

ABSTRACT

A reciprocating compressor cranktrain design is highly dependent on the definition of its connecting rod. This component, usually sintered, is designed to convert rotational movement from electrical motor into linear movement of the piston, absorb mechanism components geometrical deviations and survive the compressor envelope operating loads.

Hence, this important component fatigue behavior must be evaluated through numerical simulations, experimental bench tests and field reliability evaluations in order to predict possible failure modes caused by different operating boundary conditions characterized by the combination of bending and compression.

This work aims to explore the sintered connecting rod mechanical properties at static and dynamic combination of tensile and compressive loads. Two S-N curves with compressive and zero mean stress levels are associated to generate a fatigue criteria and calculate the connecting rod safety factor, when running within the compressor operating envelope.

Keywords: Reciprocating Compressor, Connecting Rod, Fatigue.

LIST OF FIGURES

LIST OF TABLES

LIST OF ABBREVIATIONS

LCF	Low Cycle Fatigue
HCF	High Cycle Fatigue
VHCF	Very High Cycle Fatigue
FEM	Finite Element Method
rpm	Rotations Per Minute
MSCF	Mean Stress Compensation Factor

LIST OF SYMBOLS

W	Compressor Power
Qc	Condenser Heat
Qe	Evaporator Heat
S-N	Alternating Stress vs. Cycles to Failure curve
μ	Statistical Average
σ	Statistical Standard Deviation
R^2	Coefficient of Determination for a Linear Fit
$[M]$	FEM Mass Matrix
$[\ddot{u}]$	FEM Nodal Acceleration Vector
$[C]$	FEM Damping Matrix
$[\dot{u}]$	FEM Nodal Velocity Vector
$[K]$	FEM Stiffness Matrix
$[u]$	FEM Nodal Displacement Vector
$\{F(t)\}$	FEM Load Vector
σ_y	Normal Stress in direction y (axial)
τ_{yx}	Shear Stress Perpendicular to y Direction
σ_m	Mean Stress
σ_a	Alternating Stress
A	Power Law Fit Constant Coefficient
b	Power Law Fit Exponential Coefficient
d	Step Stress for Staircase Method
μ_s	Statistical Average for Staircase Method
σ_s	Statistical Standard Deviation for Staircase Method
β	Weibull Inverse Power Law β parameter
K	Weibull Inverse Power Law K parameter
n	Weibull Inverse Power Law n parameter
$\sigma_{a_{mod}}$	Modified Alternating Stress, equivalent to Zero Mean Stress
Sf	Fatigue Safety Factor
Se	Fatigue Limit for Zero Mean Stress
Sy	Yield Strength

CONTENTS

1 INTRODUCTION

The adequate development of a connecting rod fatigue evaluation procedure must be well based and supported by a proper characterization of material properties and by the knowledge about the reciprocating compressor operating principles, with subsequent definition of loads and boundary conditions. As described by Gosney (1982) and Pedroso (2013), a refrigeration system, such as refrigerators, freezers and icemakers, is based on the fluids capacity of absorbing heat during evaporation. Basically, a refrigeration system consists in submitting a refrigerant gas to four thermodynamics subsequent processes: Compression, Condensation, Expansion and Evaporation, which occurs inside the Compressor, Condenser, Expansion Device and Evaporator, respectively, as represented in Figure 1 (a).

The thermodynamic cycle of a refrigeration system is represented in a pressure-enthalpy diagram of the refrigerant fluid, as indicated in Figure 1 (b).

Figure 1 - Refrigeration System (a) and Compressor thermodynamic cycle (b).

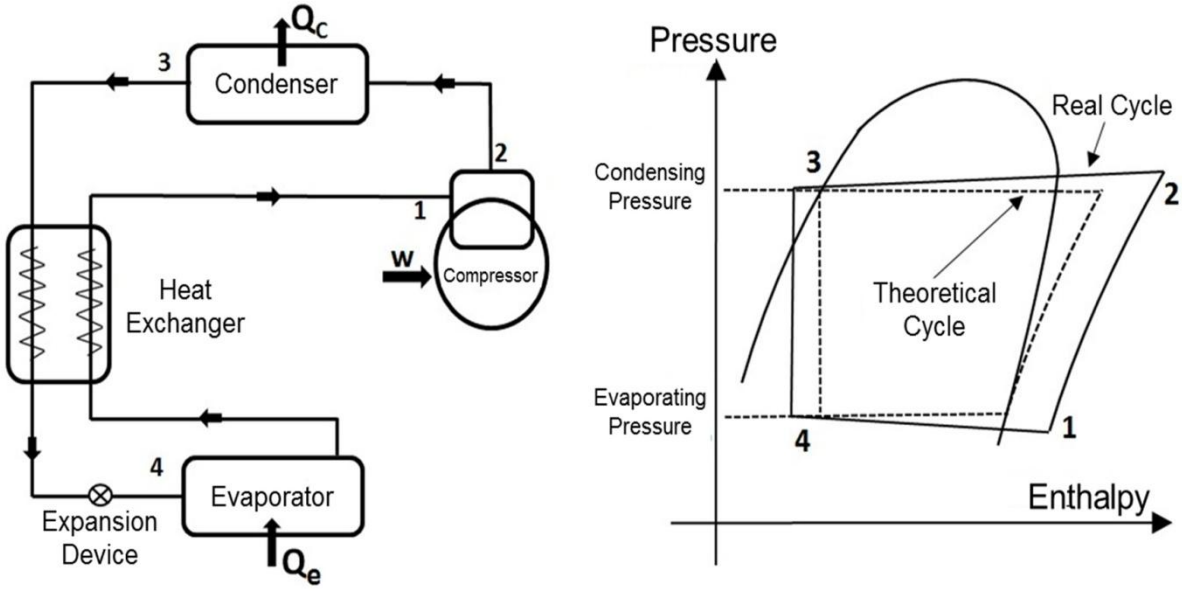

(a) (b)

Source: Pedroso (2013).

During compression (line 1-2 of Figure 1b), the vapor refrigerant suctioned by the compressor is compressed until it reaches its condensing pressure, consuming power (W). During condensing, (line 2-3), the superheated vapor with high pressure releases heat (Qc) to the ambient, changing to a liquid phase. Subsequently, the

refrigerant fluid is submitted to an expansion device (expansion valve or capillary tube) reducing its pressure to evaporation pressure (line 3-4). Finally, the refrigerant fluid passes through the evaporator (line 4-1) and removes heat (Qe) from the environment in a low pressure, causing the refrigerating effect.

As stated in Gosney (1982), the function of the compressor in a refrigerating system is to draw vapor from the evaporator, so causing a low pressure therein, at which the refrigerant can boil to give the desired temperature, and to raise the pressure of the vapor and deliver it to a condenser where the vapor can be condensed by the cooling water or cooling air.

The most common type of compressor used in refrigeration systems is the reciprocating compressor, basically composed by components indicated in Figure 2.

Figure 2 - Reciprocating Compressor components.

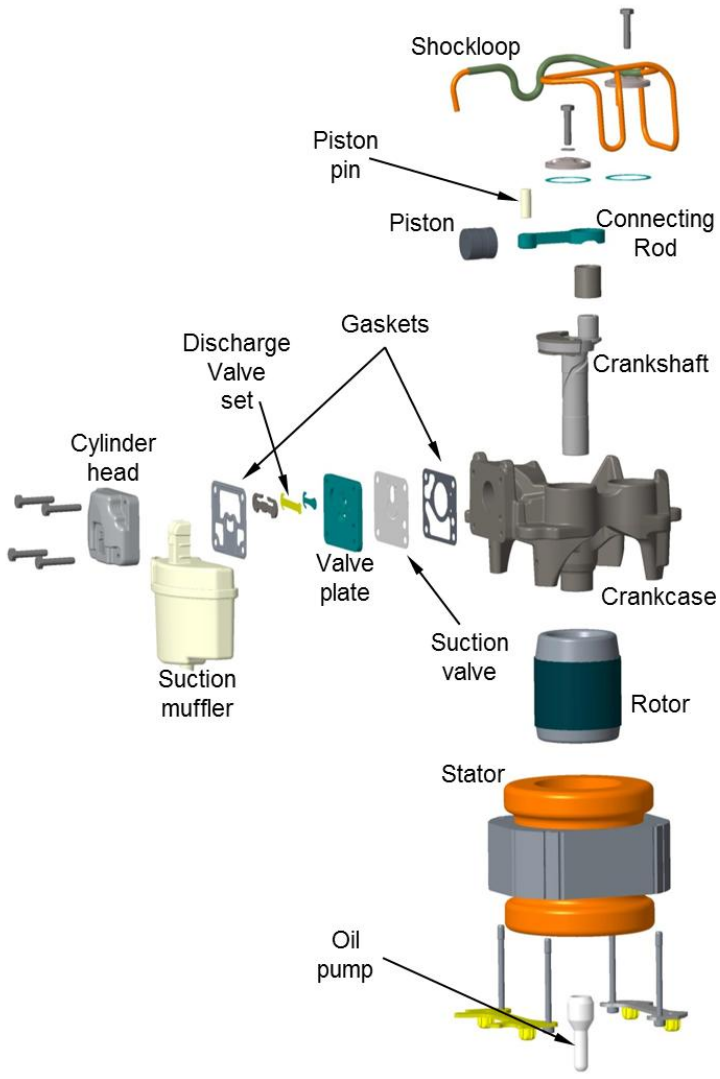

Source: Embraco

The operating principle of a reciprocating compressor is shown in Figure 3. From the rotation of the electrical motor and consequent outward movement of a piston, vapor is drawn inwards the cylinder through a suction valve which is opened automatically by the pressure difference. The vapor flows in during the suction stroke as the piston moves toward bottom dead center, filling the cylinder volume at point A with vapor at suction pressure, approximately evaporator pressure. The piston moves inwards again and the suction valve is closed by its own stiffness, trapping the vapor. The pressure then rises as the enclosed volume is reduced. This continues until the pressure inside the cylinder reaches the pressure in the discharge tube, approximately condenser pressure, point B, when the pressure inside begins to force the discharge valve open against its own stiffness. Delivery of vapor to the discharge tube continues as the piston moves on inwards to top dead center. At this point C delivery should be complete and the discharge valve closed by its own stiffness as the piston moves outwards again.

Figure 3 - Reciprocating Compressor Operating Principle.

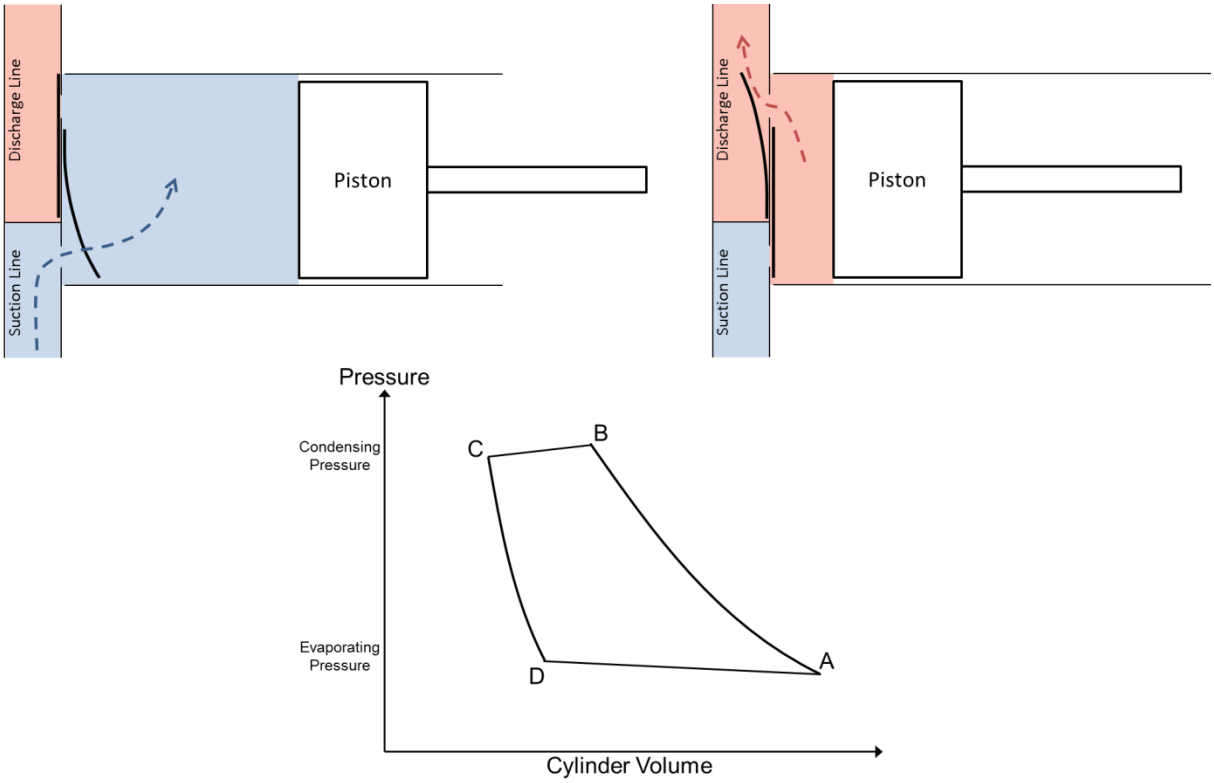

Source: Author's own figure, 2018.

A reciprocating compressor cranktrain reliability design is significantly affected by the definition of its connecting rod. This component, usually sintered, is designed to convert rotational movement from electrical motor into linear movement of the piston inside the cylinder, absorb mechanism components geometrical deviations and survive the compressor envelope operating loads. Figure 4 (a) indicates the nomenclature of cranktrain main components and Figure 4 (b) indicates specific nomenclature of Connecting Rod.

Figure 4 - Cranktrain main components (a) and connecting rod (b) nomenclatures.

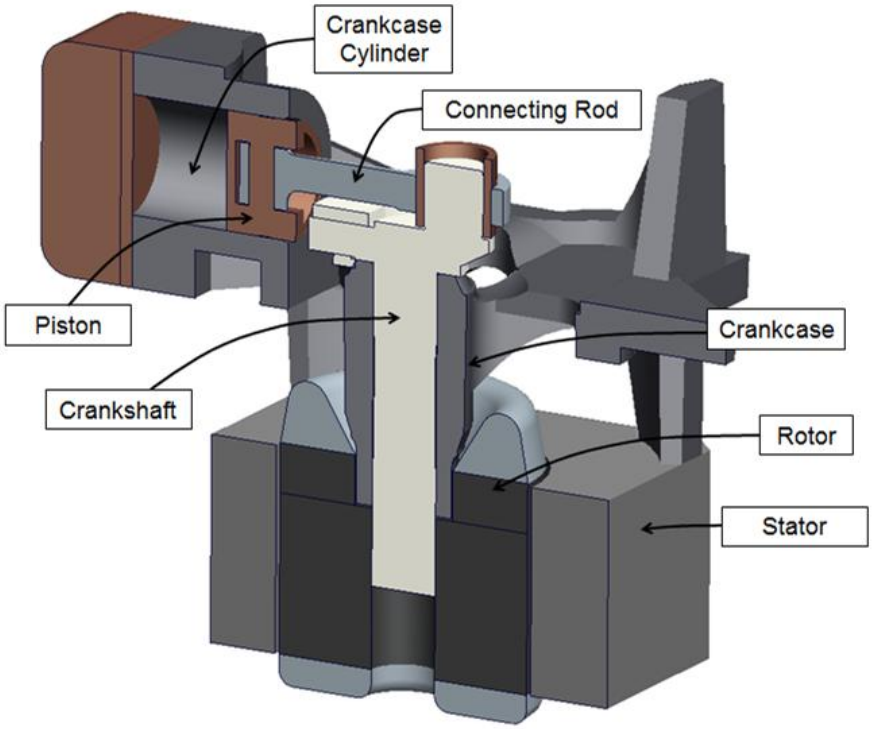

(a)

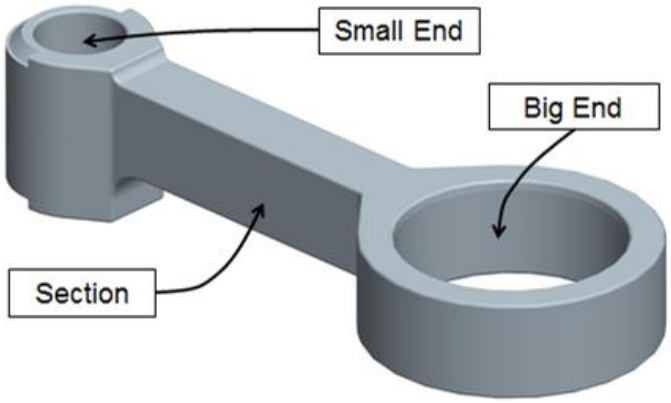

(b)

Source: Embraco

2 BACKGROUND

A reciprocating compressor is designed to operate within a working envelope, characterized by Evaporation and Condensing temperatures, measured in the refrigeration system after the expansion device and before the condenser, respectively. Depending on the operating condition, the cranktrain must run with different pressure levels, and the Pressure-Volume diagram described previously can change completely. From cranktrain analysis point of view, it is more adequate to understand the pressure levels as a function of the crankshaft angle, instead of cylinder volume. Figure 5 indicates didactically a compressor operating envelope (hatched area) and the differences between two operating pressures that a compressor must withstand, depending on the ambient temperature or thermal load inside the refrigeration system. Besides operating pressures, inner thermal profile also can change drastically.

Figure 5 - Compressor Operating Envelope.

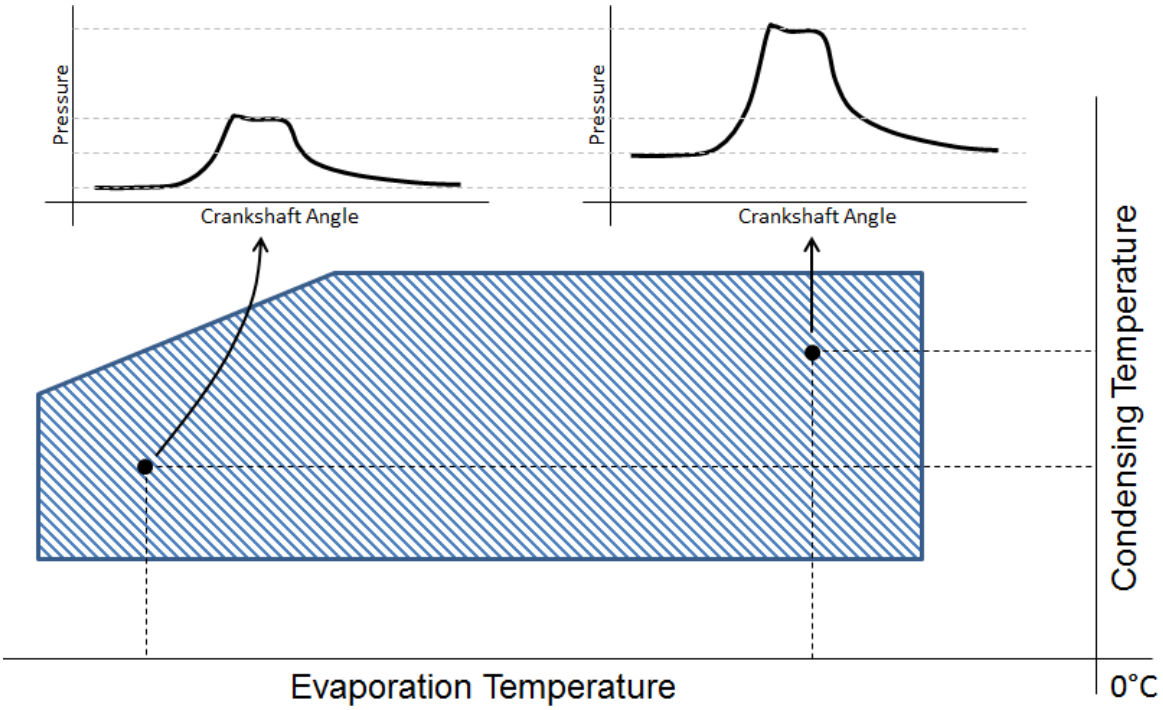

Source: Author's own figure, 2018.

The pressure applied to the piston surface is indirectly transmitted to all cranktrain components. The higher the piston area, the higher the loads causing deformation to the connecting rod and crankshaft. As a consequence, a parallelism

deviation occurs between the small and big ends of the connecting rod. Furthermore, as described in Figure 4 (b), the Connecting Rod Small End, Section and Big End are not vertically aligned. So, any compression force applied to the connecting rod extremities cause higher normal stresses on the lower side of the Section than on upper side of the Section, which characterizes bending stresses to the Connecting Rod. The same phenomenon occurs whenever the Connecting Rod is subjected to tensile loads.

Hence, this important component fatigue behavior must be evaluated through numerical simulations, static experimental and field reliability tests in order to predict possible failure modes caused by different operating boundary conditions characterized by the combination of bending and compression.

3 ASSUMPTIONS

The adequate Connecting Rod development procedure becomes even more critical each day, when new alloys and new materials are available to be used in components that require cost reduction and shorter approval time. Henceforth, the component fatigue approval including the whole refrigeration system, although more accurate, is not feasible. Besides expensive, it is impossible to isolate a single failure mode when tested in critical operating conditions.

Accordingly, a combination of bench test and numerical tools is the fastest and best alternative to evaluate a specific requirement, provided that the bench device and the numerical model are able to reproduce operating conditions and failure modes properly. The use of standard specimens on bench tests has the advantage of being applicable for any component geometry, since it evaluates the material properties itself. On the other hand, a bench test using final component provides more accurate results for an specific geometry due to considerations about correspondent notch, shape and size factors, but it can not be applied to other geometry concepts.

Although a complete test considering the compressor and it's system is always run before the compressor approval, the proposed methodology anticipates results regarding connecting rod reliability with standard specimens and bench tests, bringing a huge benefit to approval plan cost and time.

4 OBJECTIVES

4.1 General Objective

Validate a Connecting Rod fatigue behavior evaluation methodology to be used as inputs to a Safety Factors Database for an engineering company. The methodology is useful to compose geometry optimization tools, especially when dealing with new material developments.

4.2 SPECIFIC OBJECTIVES:

Apply Finite Element method through commercial software (ANSYS) to numerically describe the cranktrain operating loads for each compressor temperature condition, with focus on connecting rod operating boundary conditions.

Characterize mechanical properties of sintered material through static and dynamic bench tests. Construct Alternating Stress vs. Cycles To Failure curves for two different mean stress levels to be able to estimate the conventional fatigue limit for any other mean stress level within the evaluated range.

Define design approval criteria and calculate component fatigue and Yield Safety Factor associated to compressor main operating conditions.

Characterize Connecting Rod failure modes through visual inspections.

5 LITERATURE REVIEW:

Powder metallurgy materials offer great potential for mass production of complex-shaped components with high precision (Danninger, 2002). It is an adequate manufacturing process to produce near-net shape components at very low cost, with little wastage and alloying additions such as Mo, Mn, Cu, and Ni (Polasik, 2012). For that reason, many compressor components are produced from sinter material, including valve plate, piston and connecting rod, the focus of the present work.

The connecting rod manufacturing process usually follows a sequence of powder development, alloying addition, compaction, sintering, calibration and further surface treatments (Wheatley, 1963). Small and Big ends machining are an alternative, but not a standard.

Sintered ferrous materials are typically characterized by a porous and heterogeneous microstructure which develops from incomplete diffusion of alloying elements during sintering. Due to the incomplete diffusion of alloying elements, multiple phases are formed (Polasik, 2002), which is detrimental to the fatigue properties of powder metal parts. The nature of the porosity is controlled by several processing parameters such as compaction pressure, sintering temperature and holding time. The adequate process control is very important since the particle size, morphology, density and porosity distribution significantly affects the final component fatigue behavior (Yan, 2013).

Understanding fatigue behavior is important during performance optimization aiming weight reduction or material modification (Tiwari, 2014). The fatigue behavior is usually classified as Low Cycle Fatigue, High Cycle Fatigue or Very High Cycle Fatigue, depending on the material Stress-Life curve and the loads to which the component is subjected.

According to Polasik (2001), in high cycle fatigue regime (HCF), damage parameters and plastic strain amplitude remains relatively unchanged since the local stresses and strains are more elastic than in the low cycle fatigue (LCF) regime.

In the LCF regime, cracks initiate very early (15% of life) and the majority of the fatigue life is spent in crack propagation, while in HCF, about 80% of the fatigue life is spent initiating the crack (Polasik, 2002). Concomitantly, Polasik (2001) states that the fraction of the life required to initiate a fatigue crack tends to increase with a

decrease in fatigue stress amplitude. Thus, crack initiation occurs early in the life of LCF specimens and crack propagation mechanisms, such as deflection due to microstructural features, are more significant. In contrast, since crack initiation occupies a much higher fraction of fatigue life in the HCF regime, porosity has a more predominant effect in this regime.

Reciprocating compressor connecting rod design is mainly based on HCF and VHCF regimes. Running at high frequencies, the cranktrain life reaches 10^7 cycles very early, so the connecting rod stress levels must be safely below the fatigue limits of the material. However, in some compressor application, including liquid compression, the LCF must be considered to avoid abrupt damage increase, especially if regarding some new sintered alloy with low fatigue limit.

According to Polasik (2002), a sintered material subjected to a given strain can withstand a higher peak stress in compression than that in tension. This is attributed to the inability of pores to transfer load in tension, while in compression, local collapse of the pores and a higher degree of load transfer to the sintered regions can take place.

Fatigue life is longer for higher sintered density samples. The other contributing factor to the higher fatigue life could be the pore morphology at the initiation site which was determined by the specific shape factor of the crack initiating pore cluster (Yan, 2013).

As the porosity of a compact is increased, ductility and tensile strength are expected to decrease, especially due to the notching effect of the pores (Wheatley, 1963). A similar conclusion was registered by Yan (2013), stating that stress concentration on the sharp corner plays a significant role on the fatigue endurance limit.

On the other hand, Wheatley (1963) states that the presence of residual porosity does not have any sudden effect on the fatigue strength, but reduces it gradually in a similar way to the effect on tensile strength. This implies that the effect of the pores is simply to reduce the cross-sectional area of metal through which the crack has to grow, with the stress-concentration effects of the pores being negligible during growth in relation to the stress-concentration effects of the fatigue crack itself.

Moreover, porosity clearly decreases the Young Modulus over that of wrought alloy steel. Macroscopic ductility due to strain localization of the sintered neck regions is also significantly lower than that of most fully dense wrought alloys (Polasik, 2002).

Recent conclusions from J. M. Wheatley (1963) confirms that the Young's modulus falls with decreasing density, but Poisson's ratio is unaltered by increasing porosity. Valuable information about material behavior can be obtained using Scanning Electronic Microscopy (SEM) techniques, as shown by Yan (2013) through evaluations of different sections of a connecting rod to compare density, grain size and pores between surface and interior.

An additional remarkable characteristic of powder metallurgy is related to crack initiation occurrence at pores or pore clusters located at or near the surface of the specimen. Polasik (2002) mentions that the relatively high stress concentration at pores, particularly surface pores, is responsible for localized slip leading to crack initiation. Henceforth, an angular pore creates a higher stress concentration and stress-intensity factor than a round pore.

With regard to the possibility of internal crack nucleation, J. M. Wheatley (1963) assert that the total interior surface area of the pores is much greater than that of the free surface of the specimen and in addition to some stress-concentration effects associated with the pores, there is a tendency of promoting internal-crack nucleation. However, the length of crack that could be nucleated on the surface of an internal pore would be much lower than that on the free surface and this would probably render the initiation process more difficult. Furthermore, cracks forming and growing on the surfaces of closed pores would do so under different environmental conditions and their growth rate would probably be lower than that at a free surface in the presence of oxygen, water vapor, and other gases in the atmosphere.

Metallographic observations from Wheatley (1963) confirm that fatigue cracks start from the external free surface and propagate in a mixed transgranular and intergranular fashion from pore to pore. Previous reports from Polasik (2002) stated that after a fatigue crack has initiated at surface or subsurface pores, it tends to propagate and grow through the interpore ligaments, using pores as linkage sites. Still using SEM, Straffelini (2014) observed that the fractured surfaces actually highlight the presence of a ductile but very localized type of fracture.

Regarding a compressor connecting rod, crack initiation location depends on the kind of loads the component is subjected to. Anusha (2013) and Ambrish et al (2014) agree that the major stresses induced over the connecting rod are a combination of axial and bending stresses during operation. The axial stresses are produced due to cylinder gas pressure (compressive only) and the inertia force

arising on account of reciprocating action (both tensile as well as compressive). Bending stresses depend on the bending moment, which is a function of the vertical misalignments of Big and Small Ends, load at the Gravity Center normal to the connecting rod axis, as well as angular acceleration and linear acceleration component, normal to the connecting rod axis.

As reported by Ambrish et al (2014), there is considerable difference in the structural behavior of the connecting rod between axial fatigue loading and service operating condition. There are also differences in the analytical results obtained from fatigue loading simulated by applying loads directly to the connecting rod and from fatigue loading with the pins and interferences modeled. In addition, it was also found by Yan (2013) that the loading condition affected the fatigue endurance limit, being the fatigue endurance limit about 2.8 times higher in the bending condition than the fatigue limit obtained by axial loading. Henceforth, dynamic loads must be incorporated directly during design and optimization as the design loads, rather than using static loads.

Several experimental procedures options might be used to determine the fatigue behavior of a sintered material. Details such as load type, load profile, test frequency, test temperature, specimen geometry, specimens quantity and statistical evaluation must be cautiously defined in order to induce boundary conditions and properly reproduce the real failure mode.

To avoid excessive heating of the specimens due to dissipation effects, Godež (2014) performed bench tests at the loading frequency f = 10 Hz, because cooling of the specimens was not possible. Alternatively, G. T. Brown (1973) tested real connecting rods subjected to zero mean load at frequency of 120Hz, even without samples cooling. J. M. Wheatley (1963) concluded that the fatigue behavior also depends on the testing frequency. Considerable displacement of the S-N curve is produced by the decreased testing frequency, the average decrease in life being of the order of fifty times. It is, then, coherent to carry out the fatigue tests at temperature and frequency as close as possible to the real application, always that possible and feasible.

Yan (2013) conducted LCF tests using constant strain control, sinewave, frequency 1Hz and R=1, at room temperature, while HCF tests were conducted using constant stress amplitude control, sinewave, frequency 10Hz and R=0.1, at room temperature. Using a different strategy, Straffelini (2014) estimated the damage

accumulation with fatigue cycling adopting load blocks of 5000 cycles at a frequency of 5 Hz followed by one cycle at a frequency of 0.0025 Hz to allow a reliable Young's modulus evaluation. Those changes in Young's modulus as a function of tensile strain or cycling loading were also investigated by Straffelini (2014), indicating the importance of the knowledge if the component is under HCF or LCF.

Many current works, including (Kazymyrovych, 2009) and (Ruben, 2010) indicates that, in Low and High Cycle Fatigue regime, fatigue cracks are originated from surfaces while failures in Very High Cycle Fatigue are caused by internal inclusions. Figure 6 didactically shows the transition between HCF and VHCF for steel and aluminum materials. It is expected that the sintered material has a similar behavior.

Figure 6 - Transition between Low , High and Very High Cycle Fatigue.

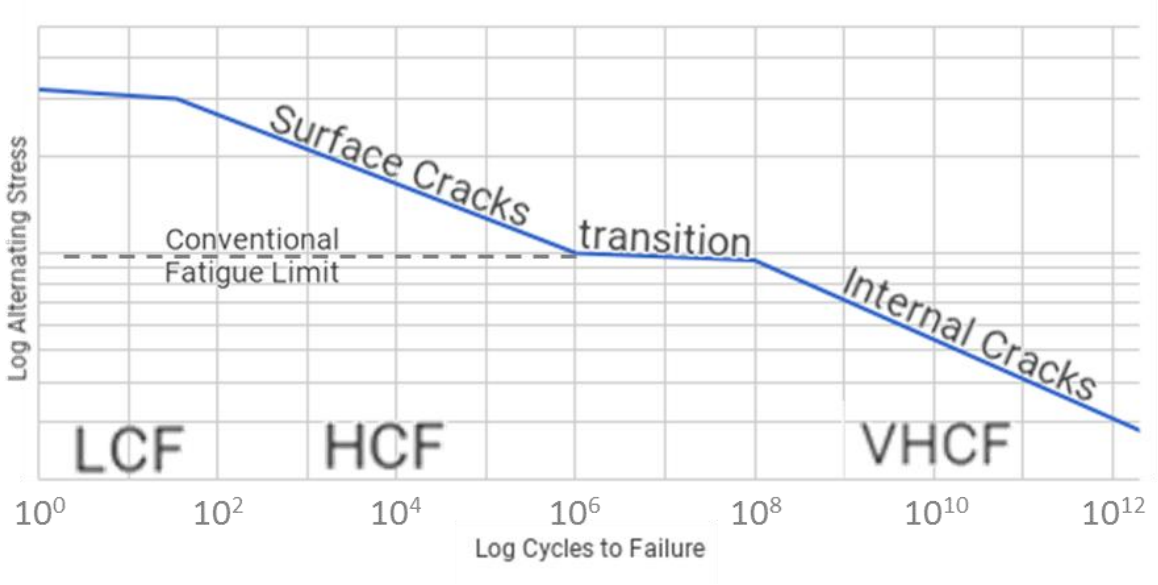

Source: Author's own figure, adapted from Kazymyrovych (2009).

In reality, conventional fatigue limit is not likely to be a horizontal line in the log log chart. However, the real decreasing inclination should be evaluated with several long duration tests, what would make the present work unfeasible. Therefore, HCF conventional fatigue limit is adopted, but conservatively considers the lower bound of confidence interval. Operating loads are relatively lower than material Yield strength and real component must withstand much more than 10^6 cycles, so no hardening is taken into account and experimental tests are controlled by stress, instead of strain.

6 METHODOLOGY

The proposed methodology to evaluate the connecting rod fatigue safety factor begins with its material mechanical properties characterization. Through experimental quasi-static tests with standard specimen in bench tests it is possible to measure the Young Modulus, Yield Stress, ultimate strength and maximum elongation during tension and compression. The material density can be simply calculated by the relation between its weight and volume. As previously stated, Poisson coefficient is very similar between similar sintered materials, so reference values can be used based on similar known sintered materials.

From those inputs, an elastic linear FEM simulation is run based on the compressor boundary conditions of each main application. Maximum and minimum principal stresses results over the connecting rod surface describes the stress profile which each connecting rod node is submitted to during one cycle. The stress profile is represented as mean and alternating stresses along time, and it can be used to calculate a fatigue safety factor, based on the material fatigue limit and an adequate fatigue criteria.

Subsequently, dynamic axial tests controlled by sinusoidal tensile-compressive loads are used to investigate the Stress-Cycles curves of material for two different mean stress levels, close to the component real application. From this point it is possible to estimate the material surface fatigue limit for each mean stress, define a relation between different mean stresses and calculate the safety factor for the application described through numerical simulations.

Figure 7 illustrates the methodology applied to evaluate the reciprocating compressor connecting rod fatigue safety factor.

Figure 7 - Connecting rod fatigue evaluation methodology

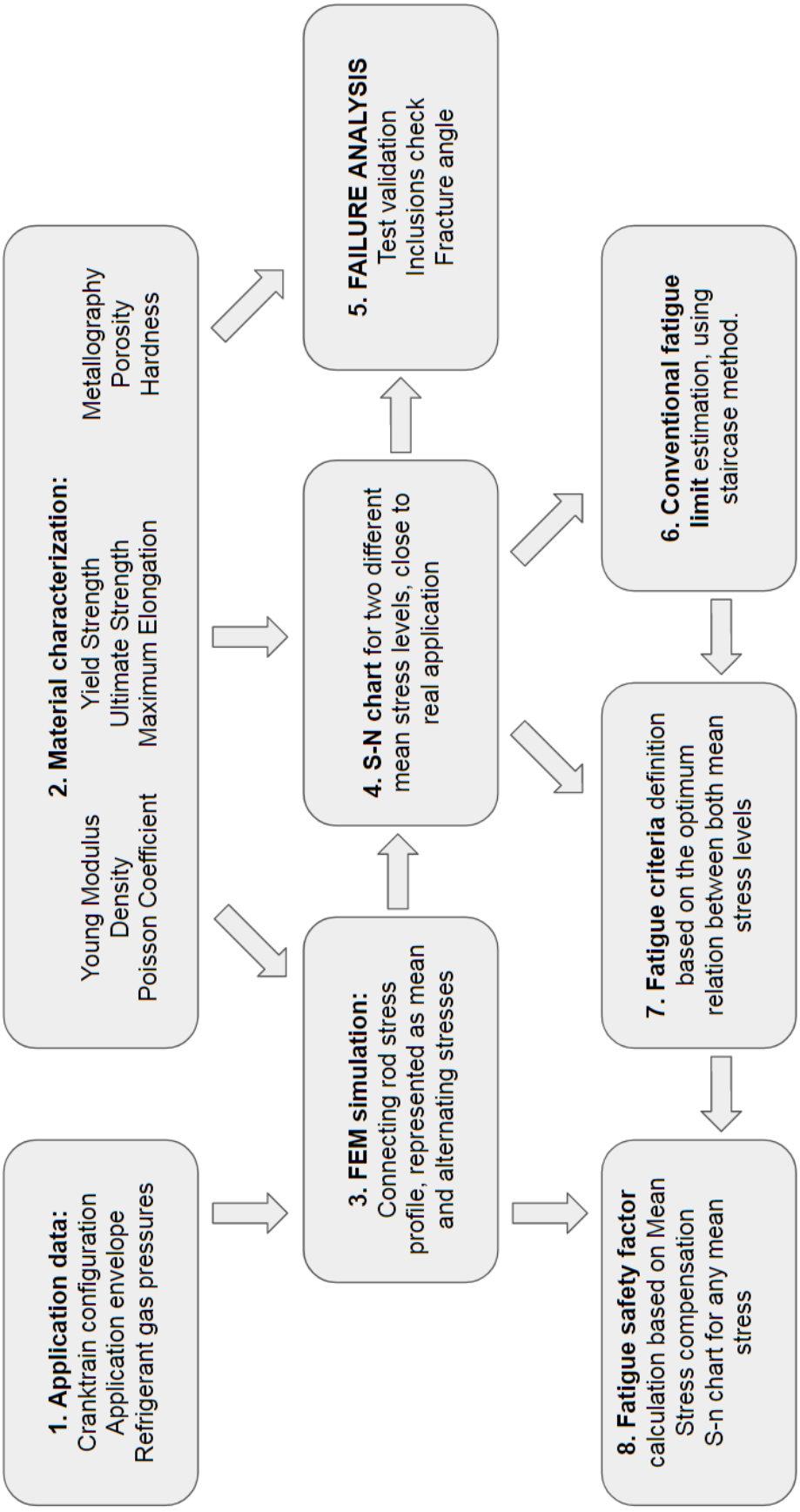

Source: Author's own figure, 2018.

6.1 APLICATION DATA

For each compressor application and temperature envelope, there are main operating conditions that can approximately represent the entire life of the compressor, usually classified as one more severe 1st condition, during 10% of the time, an intermediate 2nd condition, during 60% of the time and a softer 3rd condition, during 30% of the time.

Compressor performance requirements (capacity and efficiency within the temperature envelope) are achieved depending on cranktrain characteristics as piston diameter and crankshaft eccentricity, refrigerant gas properties, manifold configuration and motor design. Figure 8 shows the theoretical chart of cylinder pressure vs. crankshaft angle for a confidential cranktrain configuration running at 3 main operating conditions.

Figure 8 - Cylinder pressure vs. crankshaft angle at 3 main operating conditions.

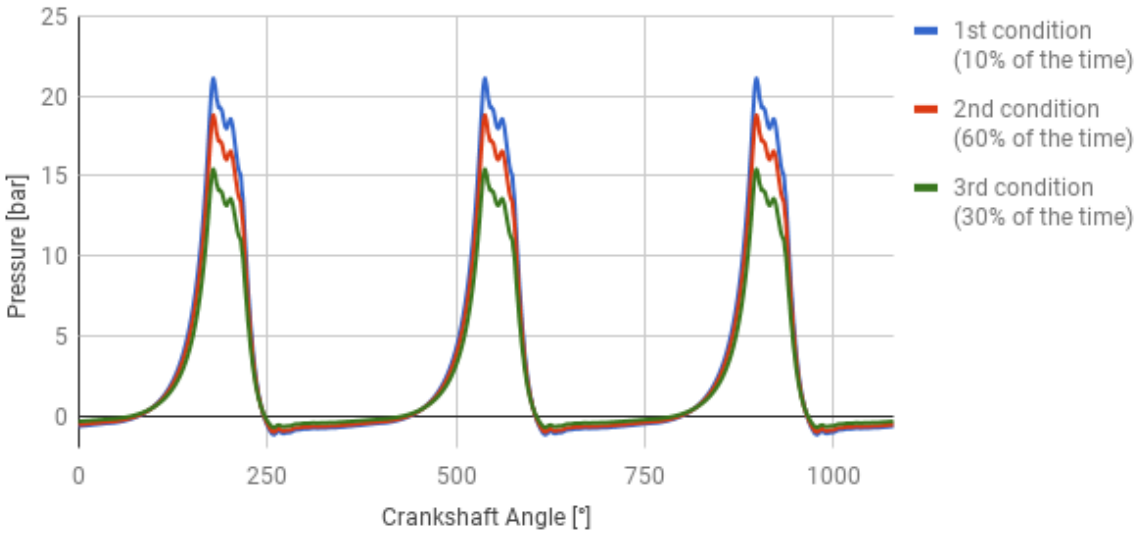

Source: Author's own figure, 2018.

With regard to connecting rod design, the chart from figure 8 is used as input for many important evaluations, as bearings simulation to define Big End and Small End radial clearances, connecting rod flexibility simulation to guide the piston aligned through the cylinder bearing, and connecting rod fatigue analysis to survive the operating loads. Fatigue analysis is the focus of the present work and will use chart from figure 8 as input for numerical FEM evaluations, discussed in next topics.

6.2 MATERIAL CHARACTERIZATION

The connecting rod sintered material under evaluation is basically composed by Fe + 0.5%Si + 4%Ni +6.5%vo. C +1%vol. hBN + 0.8% Lube-E. After blending, compaction occurs at pressure 600 MPa and sintering process is made at 1120°C during 1 hour (5°C/min) at controlled atmosphere of 95% argon and 5% hydrogen. This process generates an alloy with Brinell hardness 123 ± 10 HB5 (5 samples measured) and metallography described in Figures 9 and 10.

Figure 9 - Metallography without chemical attack, magnification 50x (a) and 100x (b).

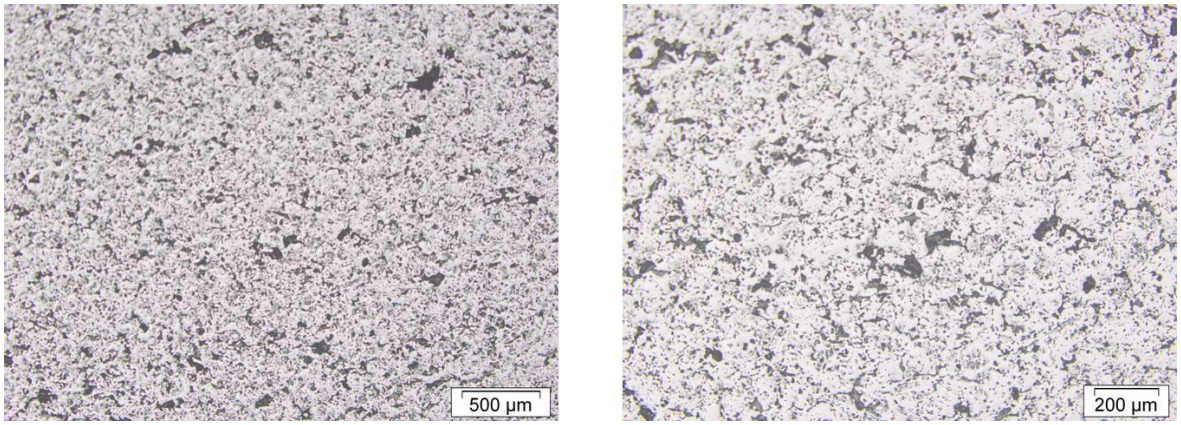

(a) (b)

Source: Technical analysis from partnership between UFSC and Embraco materials laboratories.

Figure 10 - Polishing and chemical attack metallography, magnification 200x (a) and 1000x (b).

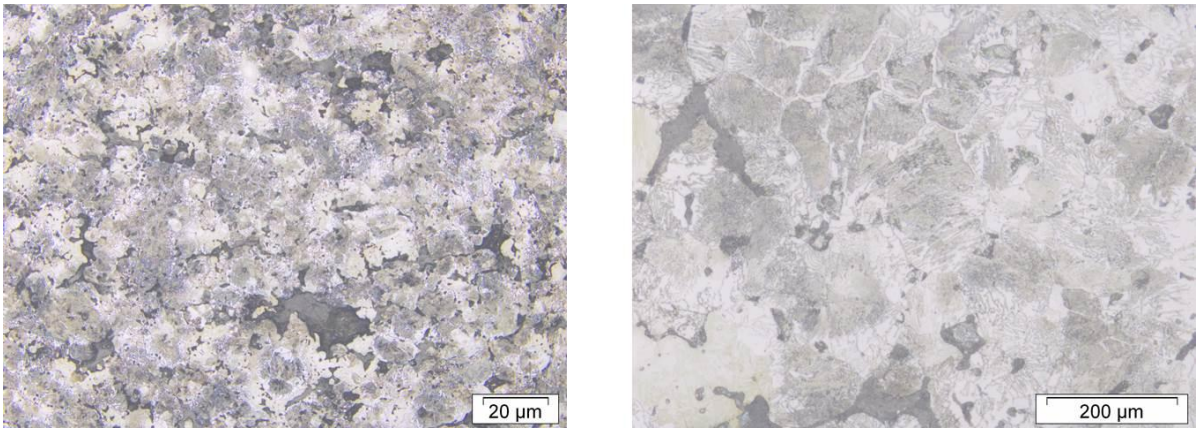

(a) (b)

Source: Technical analysis from partnership between UFSC and Embraco materials laboratories.

By way of comparison with similar alloys, evidential porosity evaluation is summarized for 4 different samples in Figure 11. However, the porosity evaluation is very sensitive to sample polishing preparation and presence of discontinuities. Consequently, dark regions of Figure 11 (a) represents material porosity added to solid lubricant, which may slightly deviate from actual porosity result, graphically registered in Figure 11 (b).

Figure 11 - Sintered material porosity evaluation with magnification 100X.

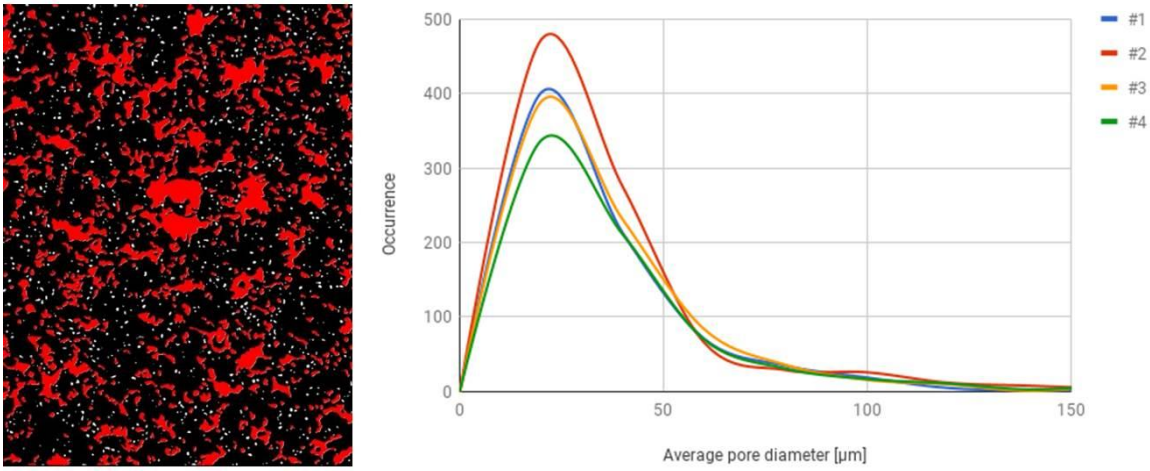

Source: Technical analysis from partnership between UFSC and Embraco materials laboratories.

It is known that the porosity, hardness and even mechanical properties are not homogeneous for the standard specimen, much less for the real connecting rod. However, the present work considers homogeneous characteristics as a simplification.

In a detailed reliability analysis description from SAE Handbook (1997), it is stated that a fundamental requirement for any durability assessment is knowledge of the relationship between stress and strain and an estimation of fatigue limit level for the material under consideration. Fatigue is a highly localized phenomenon that depends very heavily on the stress and strain experienced in critical regions of a component or structure. The relationship between uniaxial stress and strain for a given material is unique, consistent and, in most cases, largely independent of location. Therefore, a standard specimen tested under axial conditions in laboratory can be used to adequately represent the behavior of a component of the same material at a critical location.

Thus, quasi-static axial tests must be performed to obtain materials information such as Young Modulus, Yield stress, ultimate strength and maximum elongation during tension and compression.

Swedish standard SIS 11 21 23, corresponding to ISO2740, specifies the die cavity dimensions used for making tensile test pieces by pressing and sintering. Figure 12 indicates the required specimen dimensions in millimeters, chosen based on similarities with the real connecting rod component rectangular cross section.

Figure 12 - Standard specimen for axial quasi-static tests, according to Swedish SIS 11 21 23.

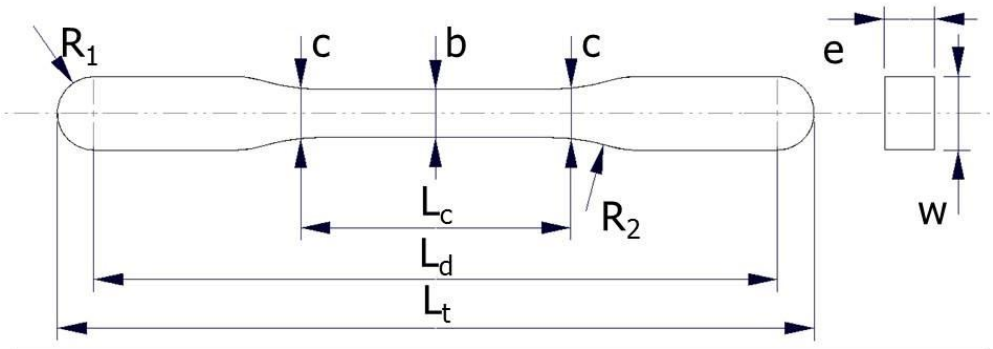

b	c	L_c	L_d	L_t	w	e	R_1	R_2
5.70	5.95	32.0	81.0	89.7	8.70	6.00	4.35	25

Source: Swedish SIS 11 21 23.

Sharp edges as a result of the pressing must be grinded, so that the the production process of the standard specimen is the same from the real connecting rod and the surface finishing should be very similar.

Quasi-static axial tests to characterize the relation between strain and stress require a calibrated load cell and strain gage. During the present work, it was used a MTS 810 Material Test System for axial tests, equipped with load cell calibrated up to 10KN, 647 hydraulic wedge grip fixation pressure 1 Kpsi and operating oil flow 15 gallon per minute. Clipgage model 632.11C-20 with maximum grid 25.4mm was attached to the standard specimen to monitor test strain. Figure 13 (a), (b) and (c) show, respectively, MTS, Clipgage and fixation procedure used to execute the experimental static tests.

Figure 13 – MTS (a) and Clipgage (b) used to execute experimental tests.

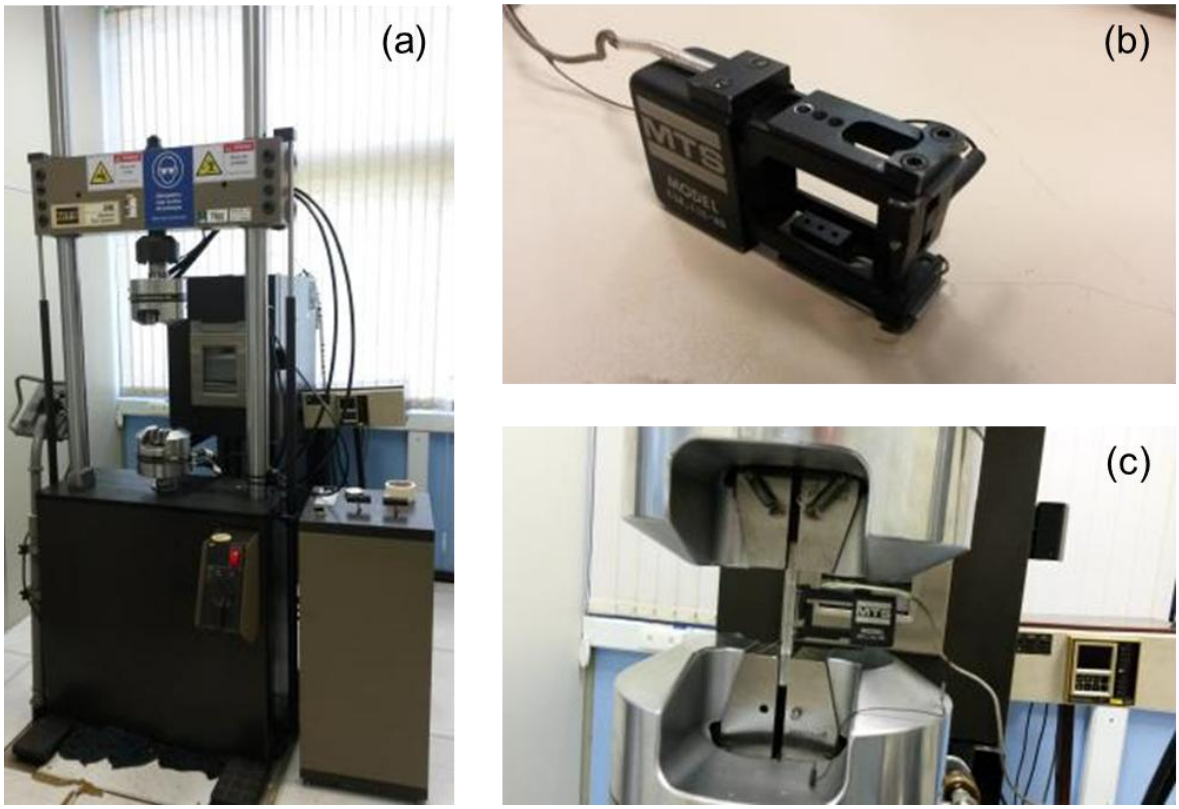

Source: Author's own figure, from Embraco materials laboratory, 2018.

MTS software TestStar™ IIs Station Manager 4.0D, applies displacement at rate 0.02 mm/s registering associated load and strain at each 0.2s. Subsequently, load values are converted to stress to plot the material strain vs. stress curve. Ambient temperature was controlled between 20°C and 22°C. Figure 14 shows the results of the axial tests with 13 standard specimens, 6 with tensile and 7 with compressive loads.

Figure 14 - Strain vs. Stress curves associated to tensile and compressive loads.

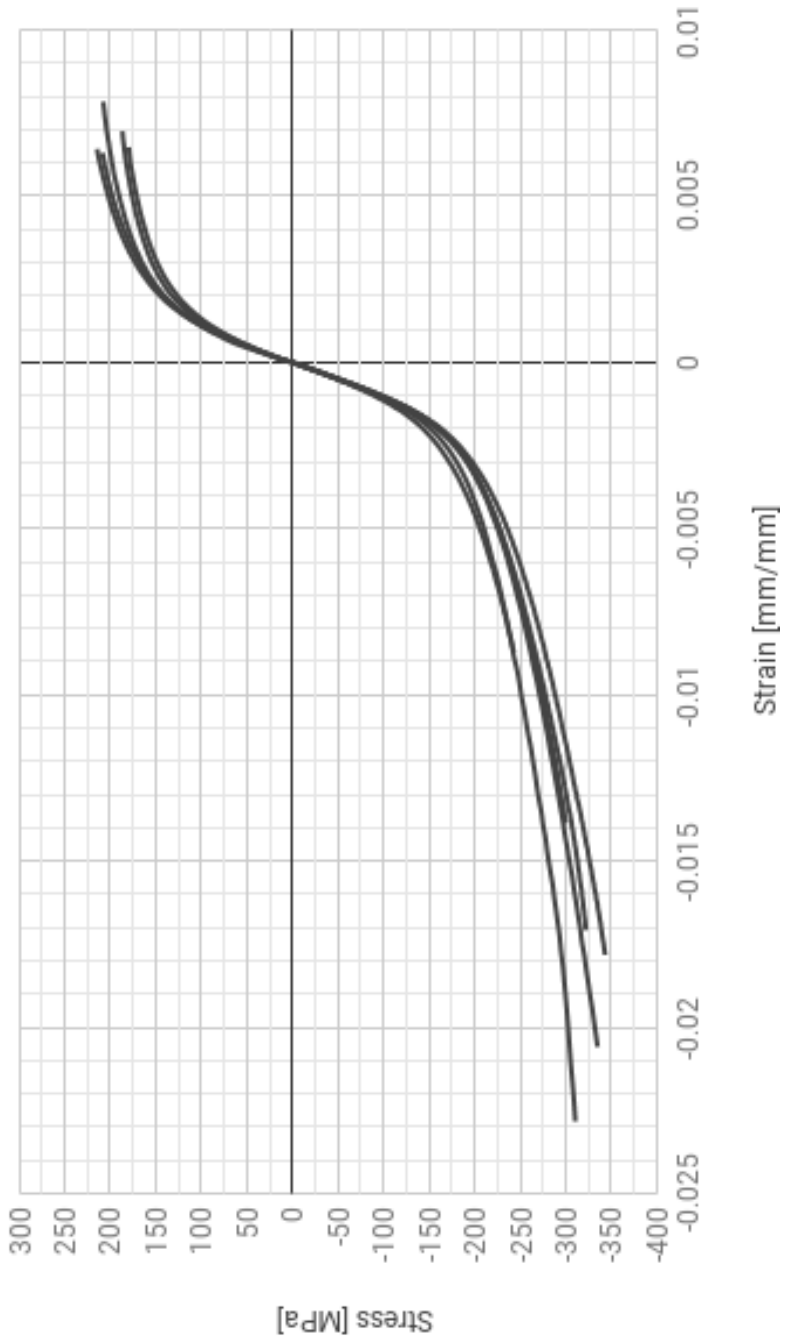

Source: Author's own figure, 2018.

Raw data for detailed analysis is registered in Tables 1 and 2. Assuming that the results are properly described by a normal distribution, 99.73% of the samples should be contained within the interval $\mu \pm 3\sigma$ (average plus-minus 3 times the standard deviation). Compressive evaluations with samples 3, 4 and 5 were not finished due to technical problems, but elastic behavior and Yield strength measurement were not affected.

Table 1 - Summary of compressive quasi-static tests.

Compressive				
#	Young Modulus [GPa]	Yield Strength [MPa]	Ultimate Strength [MPa]	Max. Elongation [mm/mm]
1	98551	-121	-310	-0.0228
2	98780	-143	-335	-0.0206
3	97868	-131	-	-
4	96124	-123	-	-
5	100321	-141	-	-
6	99574	-147	-322	-0.0171
7	102607	-140	-343	-0.0178
μ	99118	-135	-328	-0.0196
σ	2033	10	14	0.0026
μ+3σ	105216	-104	-284	-0.0117
μ-3σ	93020	-166	-371	-0.0275

Source: Author's own production, 2018.

Table 2 - Summary of tensile quasi-static tests.

Tensile				
#	Young Modulus [GPa]	Yield Strength [MPa]	Ultimate Strength [MPa]	Max. Elongation [mm/mm]
8	-	-	-	-
9	92878	104	180	0.0065
10	109543	105	208	0.0078
11	99706	111	185	0.0047
12	97484	118	208	0.0063
13	102117	117	214	0.0064
14	95237	107	187	0.0070
μ	99494	110	197	0.0065
σ	5896	6	15	0.0010
μ+3σ	117184	128	241	0.0095
μ-3σ	81805	93	152	0.0034

Source: Author's own production, 2018.

Restricting material data to exclusively linear behavior, 13 quasi-static tests are used to evaluate the material Young Modulus, since the linear region of the chart has the same inclination for tension and compression. Figure 15 shows a linearization of all data with stress lower than 75 MPa.

Figure 15 - Young Modulus determination.

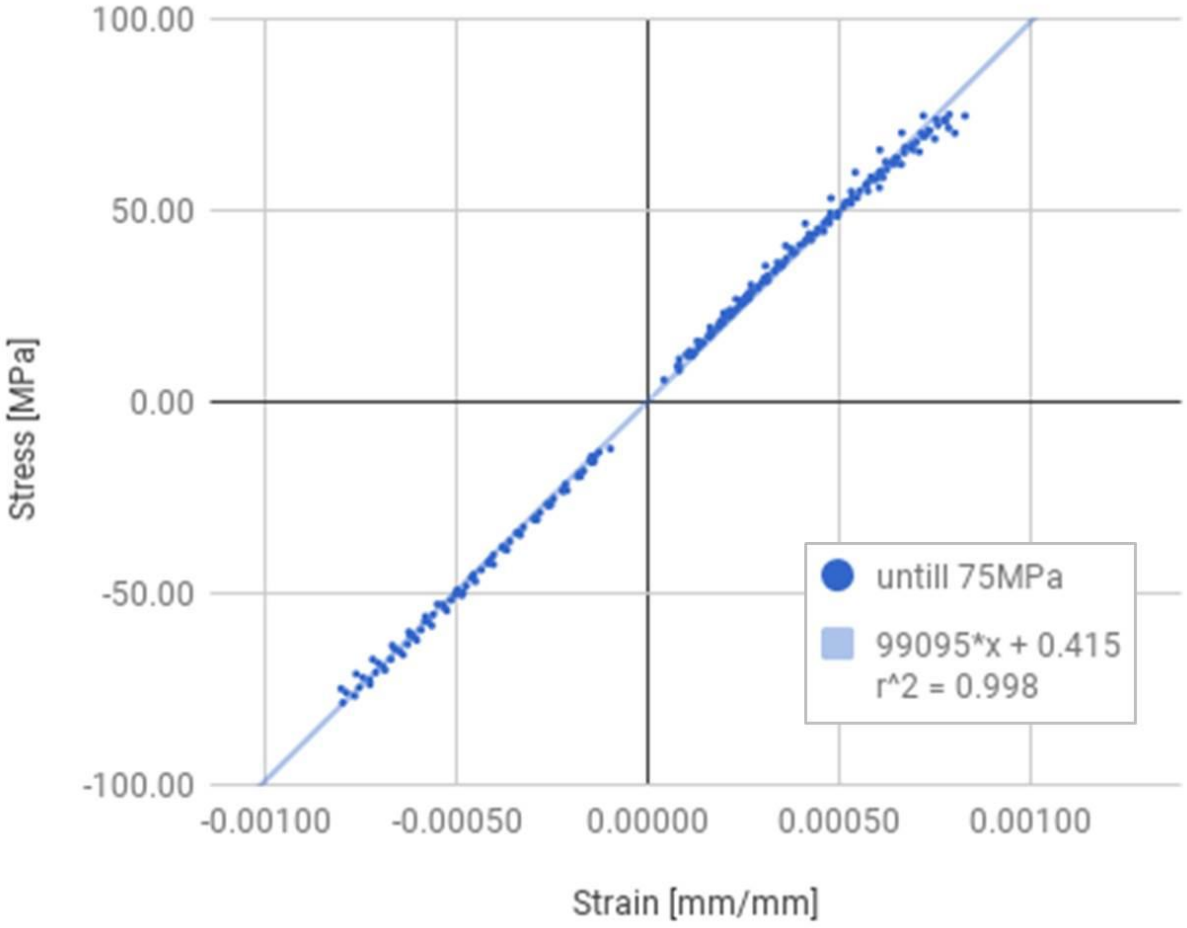

Source: Author's own figure, 2018.

Considering a linearization of all acquired data from the elastic regime, the material Young Modulus is obtained as 99 ± 12 GPa with coefficient of determination R^2=0.998. It is used as a linear elastic input for transient structural numerical simulation, described in future topic.

Other important results can be extracted from figure 14, as the Yield stress (0.2% strain) and ultimate strength. In average, material Yield stress when submitted to tension is equivalent to 110 MPa while during compressor is equivalent to 135 MPa. The ultimate strength is much higher when submitted to compression, 328 Mpa

against 197 MPa, when submitted to tension loads. This information is used to define the stress levels of the axial dynamic tests, described in future topic.

The standard specimen was also used to calculate the material density. Using a caliper rule to measure the specimen main dimensions, its volume is calculated. The relation between its weight and volume indicates average density for the sintered material 6300 ± 235 Kg/m³ (7 samples measured). It is used as an input for the transient structural FEM simulation, described in future topic. Poisson coefficient is also a requirement for future analysis, but the present work assumes it as 0.3, equivalent to similar sintered materials.

6.3 FEM SIMULATIONS

The connecting rod fatigue evaluation must be based on strain and stress cycles from the dynamic loads which the cranktrain is subjected during operation, as described in topic 6.1. A triaxial extensometer instrumentation to evaluate strain levels in a moving component during a cycle, besides too expensive, would contain a lot of errors and noise, making it impossible to accurately predict the real strain levels over the component surface.

Finite Elements Method becomes the most feasible alternative to represent the interfaces within the cranktrain, the behavior of materials and consequently the components deformation and possible failure region. The combination of pressure conditions and rotational velocities are evaluated using ANSYS Workbench 18.2 transient structural analysis through full method of Mechanical APDL iterative solver. This type of analysis is used to determine the dynamic response of a structure under the action of any general time-dependent loads. It can be used to determine the time-varying displacements, strains, stresses, and force reactions in a structure as it responds to any transient loads. The time scale of the loading is such that the inertia or damping effects are controlled by stiffness (Beta) and mass (Alpha) coefficients.

The basic equation of motion solved by the transient dynamic analysis is shown in Equation 1.

$$[M]\{\ddot{u}\} + [C]\{\dot{u}\} + [K]\{u\} = \{F(t)\} \quad (1)$$

where $[M]$ is the mass matrix, $[C]$ is the damping matrix,$[K]$ is the stiffness matrix, $\{\ddot{u}\}$ is the nodal acceleration vector, $\{\dot{u}\}$ is the nodal velocity vector, $\{u\}$ is the nodal displacement vector and $\{F(t)\}$ is the load vector.

At any given time, t, these equations can be thought of as a set of static equilibrium equations that also take into account inertia forces ($[M]\{\ddot{u}\}$) and damping forces ($[C]\{\dot{u}\}$). The ANSYS program uses the Newmark time integration to solve the equations at discrete timepoints. The time increment between successive timepoints is called the integration time step.

The Transient Structural transient analysis setup follows a basic sequence of geometry creation, material properties definition, connections coupling, mesh generation, boundary conditions appliance and results evaluation.

Cranktrain geometry, due to its complexity, must be created in more advanced CAD software, in this case, Creo Parametric 3.0 M080. Subsequently, some geometry simplifications for meshing purposes are necessary, usually using Designmodeler, from ANSYS package.

The material mechanical properties are defined as isotropic linear elastic, derive from Young Modulus and Poisson's ratio at ambient temperature, registered in topic 6.2. No plastic behavior of materials hardening is considered because no Yield is expected at the operating levels. Density is a physical property that must be considered to represent the inertia loads and is also registered in topic 6.2.

The connections among components are settled through deformable cylindrical joints added to low torsional and axial damping, representing the lubricant oil viscosity filling the clearances between the bearings. For all radial bearings, the cylindrical joints enables axial and rotational degree of freedom in an specific direction, as represented by Z axis shown in figure 16 (a) to (f). All other degrees of freedom are disabled.

Figure 16 - Joint connections representing cranktrain bearings in ANSYS.

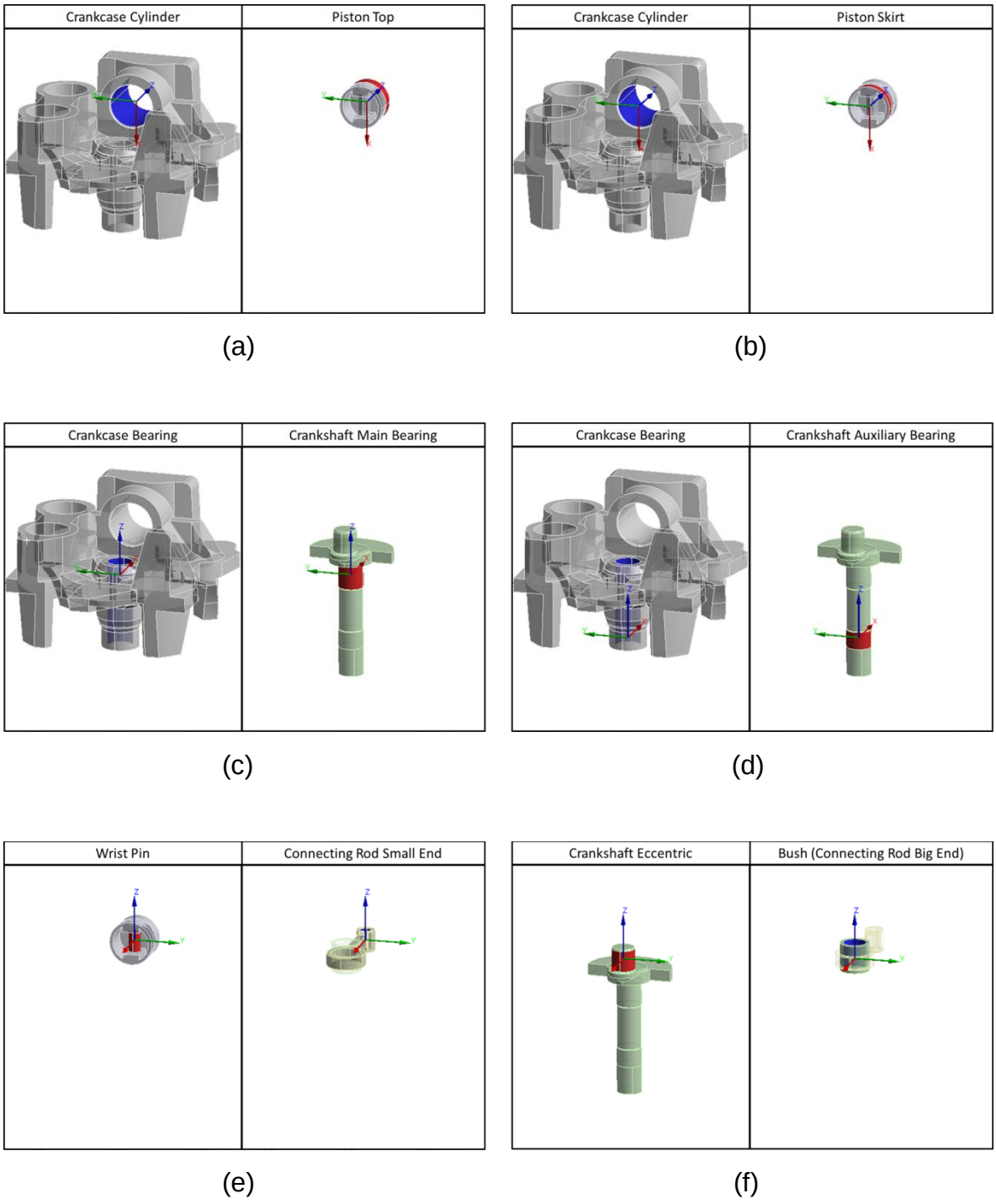

Source: Author's own figure, pictures from ANSYS Workbench 18.2, 2018.

The compressor operating boundary conditions are simplistically reproduced as normal pressure applied to piston, according to the three main application conditions described by Figure 8, equivalent counterpressure applied to Valve Plate (manifold), and constant rotation speed (3600 rpm) applied to rotor, which is attached to the crankshaft.

Through a local refinement sensitivity analysis, the Connecting Rod mesh must be defined based on a relation between result quality and computational cost, being generated with Quadratic Hex Dominant method (20 nodes for each hexahedral element). Three different connecting rod mesh sizes were evaluated: Fine (element size 1mm, generating 28831 nodes for connecting rod), Medium (size 1.6mm, generating 12835 nodes for connecting rod) and Coarse (size 2.3mm, generating 5378 nodes for connecting rod). Mesh options are shown in Figure 17 (a), (b) and (c), respectively.

The global Mesh representing the remaining cranktrain components is composed by Linear Hexahedral (8 nodes) and tetrahedral (4 nodes) elements, as shown in figure 17 (d).

Figure 17 - Finite Element Mesh representing Compressor Cranktrain in ANSYS.

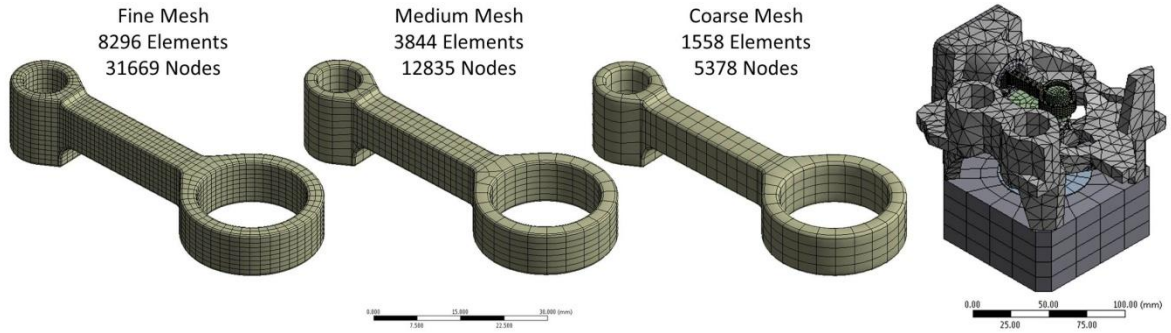

(a) (b) (c) (d)

Source: Author's own figure, 2018.

In a transient structural simulation, the adequate time step is highly influenced by the mesh element size. As a general recommendation, the time step should be sufficiently short so a vibration wave can go through the element length at the sound speed in the material environment. Hence, the smaller the element size, the lower is the time step required to properly represent the transient phenomenon. Such a short time step is not feasible for this kind of simulation, so, although the general recommendation is not fully adhered, lower time step was considered for smaller element size. Therefore, Fine mesh is associated with time step 7.04e-05s, Medium mesh is associated with time step 9.61e-05s and Coarse mesh is associated with time step 1.51e-04s.

Considering all three mesh options, minimum principal stress for a randomly chosen node close to the connecting rod small end, when running in 1st main operating condition, is plotted in Figure 18.

Figure 18 - FEM mesh sensitivity.

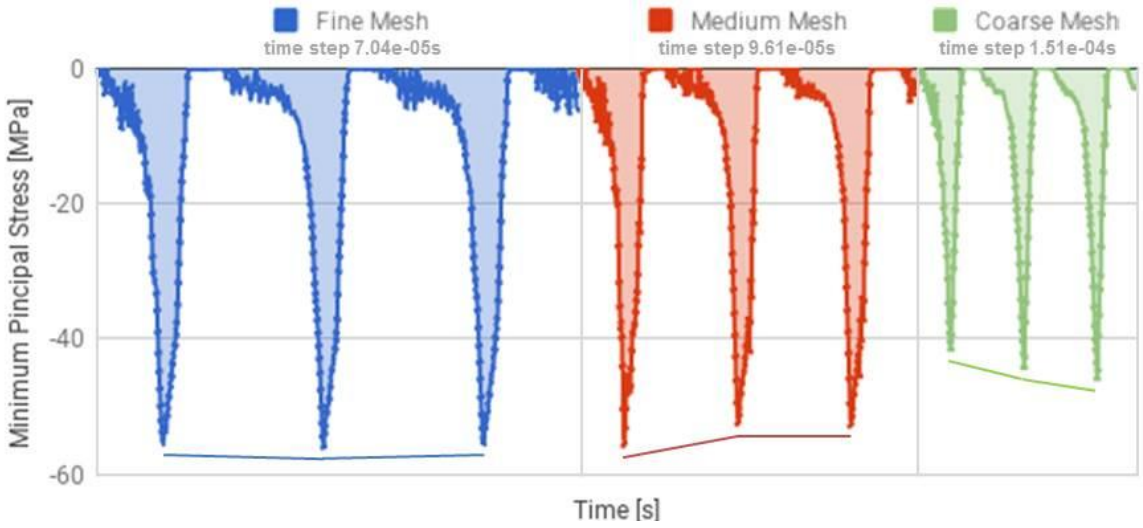

Source: Author's own figure, 2018.

It is possible to note that, although coarse mesh requires fewer substeps to complete 3 simulation cycles, the minimum principal stress results are different at each cycle, indicating that the simulation is still not converged after 3 cycles. Run additional cycles to converge the simulation would take longer than run the simulation with a finer mesh.

Medium mesh provides very similar results in cycles 2 and 3, indicating that the convergence is achieved. Furthermore, minimum values of cycles 2 and 3 are pretty similar to results obtained with Fine mesh, therefore, Medium mesh could be selected as the best option considering a relation between results and computational cost. However, the present work registers all results with Fine mesh, since it has more stable results at each cycle and total simulation time is still feasible for few runs (2 parallel runs in 10h).

Connecting rod Fine mesh, added to remaining components mesh, sums total 25129 elements and 37758 nodes.

Based on preliminary results for mesh definition, critical nodes to evaluate the fatigue life are selected according to identification A to H and location described in Table 3.

Table 3 - FEM critical nodes description.

Node	Location
A	Upper left side of small end
B	Upper left side of big end
C	Upper right side of small end
D	Upper right side of big end

Node	Location
E	Lower left side of small end
F	Lower left side of big end
G	Lower right side of small end
H	Lower right side of big end

Source: Author's own production, 2018.

Several results are available as output from the numerical simulation. For instance, Figure 19 qualitatively shows the connecting rod joints force reactions, applied to big and small end during maximum compression (a) and maximum tension (b).

Figure 19 - Connecting rod FEM joint force reactions.

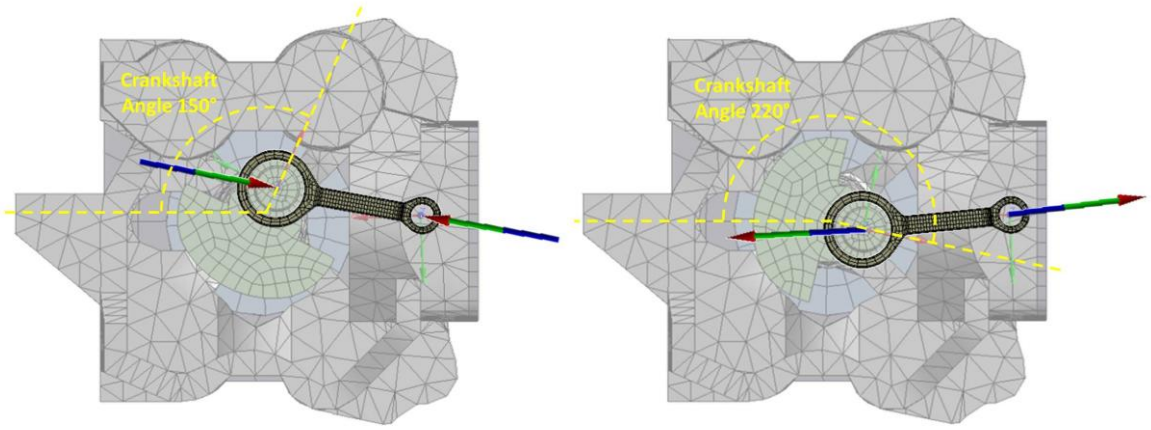

Source: Author's own figure, 2018.

Figure 20 shows a cut section of the connecting rod when submitted to compressive loads. Normal stress distribution for its axial direction (Y axis) is plotted for qualitative analysis.

Figure 20 - Connecting rod FEM normal stress distribution in direction X.

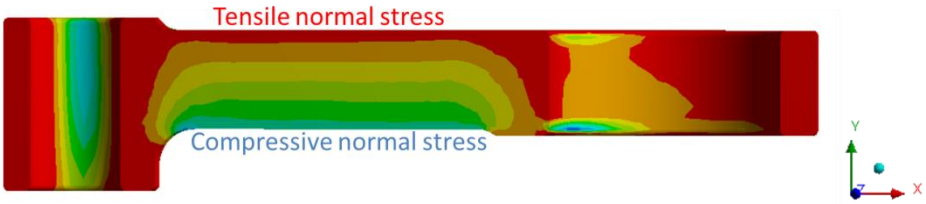

Source: Author's own figure, 2018.

It confirms the statement from Introduction section, that any compression load applied to the connecting rod extremities causes higher normal stresses on the lower side of the Section than on upper side, characterizing bending stresse.

Previous studies from Puff (2015) show that sintered materials under static bending loads have a very low notch sensitivity due to the natural presence of internal pores. It overestimates FEM stress results close to geometric discontinuities, but the author also states that the notch sensitivity for dynamic applications is relatively higher than his static evaluations. Therefore, FEM results for the present connecting rod analysis are considered acceptable due to conservative reasons.

Considering nodes from A to H, Maximum Principal Stresses, Minimum Principal Stresses and Maximum Shear Stress during compression are registered in Table 4 for the three main conditions evaluated.

Table 4 - Principal stress results for critical nodes running in main operation conditions.

	1st Main Condition			2nd Main Condition			3rd Main Condition		
Node	Min. Principal Stress [MPa]	Max. Principal Stress [MPa]	Max. Shear Stress [MPa]	Min. Principal Stress [MPa]	Max. Principal Stress [MPa]	Max. Shear Stress [MPa]	Min. Principal Stress [MPa]	Max. Principal Stress [MPa]	Max. Shear Stress [MPa]
A	-60.98	9.31	30.56	-54.82	7.65	27.47	-45.75	7.80	22.93
B	-47.07	13.06	23.66	-42.20	12.07	21.21	-35.48	14.20	17.83
C	-63.31	9.18	31.16	-56.31	10.06	27.71	-46.15	9.90	22.71
D	-38.93	7.81	19.54	-35.79	9.55	17.96	-31.17	7.42	15.64
E	-70.05	17.88	34.90	-62.36	19.80	31.06	-51.56	15.15	25.68
F	-75.68	20.31	38.43	-66.55	19.02	33.79	-54.52	17.52	27.68
G	-48.29	10.55	24.12	-42.92	13.25	21.44	-35.94	8.56	17.95
H	-83.98	12.35	42.34	-75.45	12.70	38.04	-62.93	10.67	31.73

Source: Author's own production, 2018.

Detailed results for critical nodes A, E, F and H, when running in 1st main condition, are registered in Figures 21 to 24.

Figure 21 - Principal Stresses for node A, located at upper left side of small end.

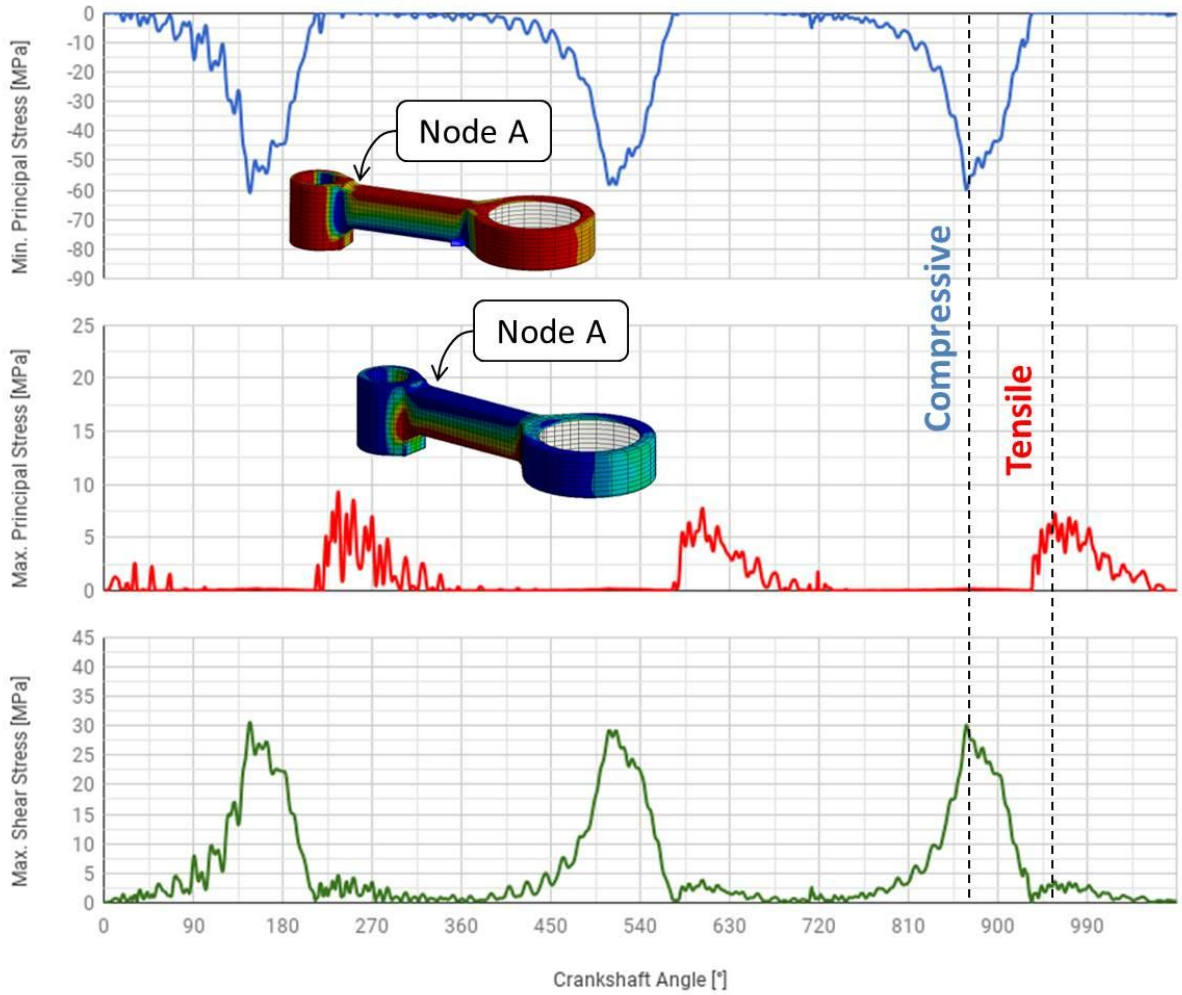

Source: Author's own figure, 2018.

Figure 22 - Principal Stresses for node E, located at lower left side of small end.

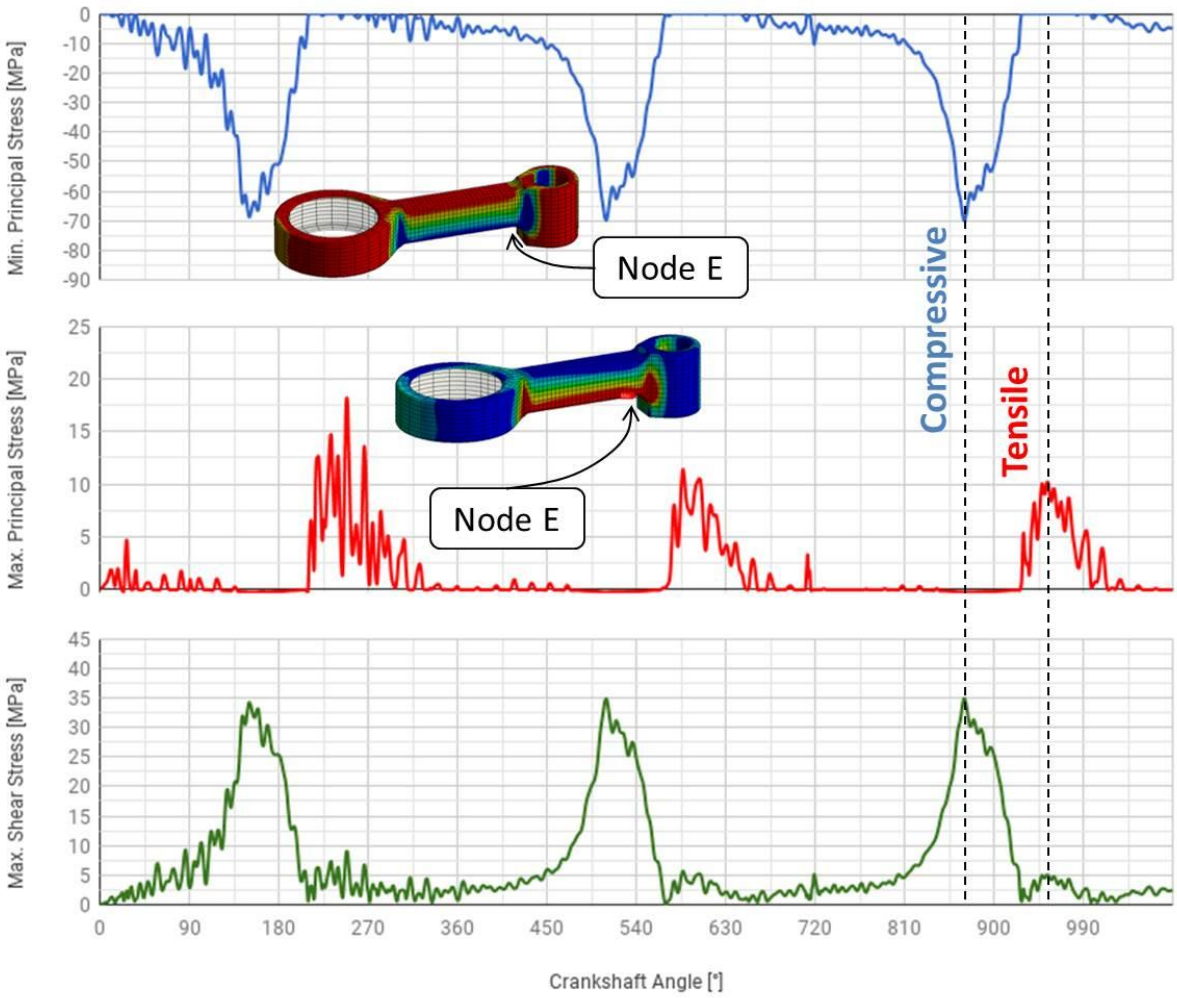

Source: Author's own figure, 2018.

Figure 23 - Principal Stresses for node F, located at lower left side of big end.

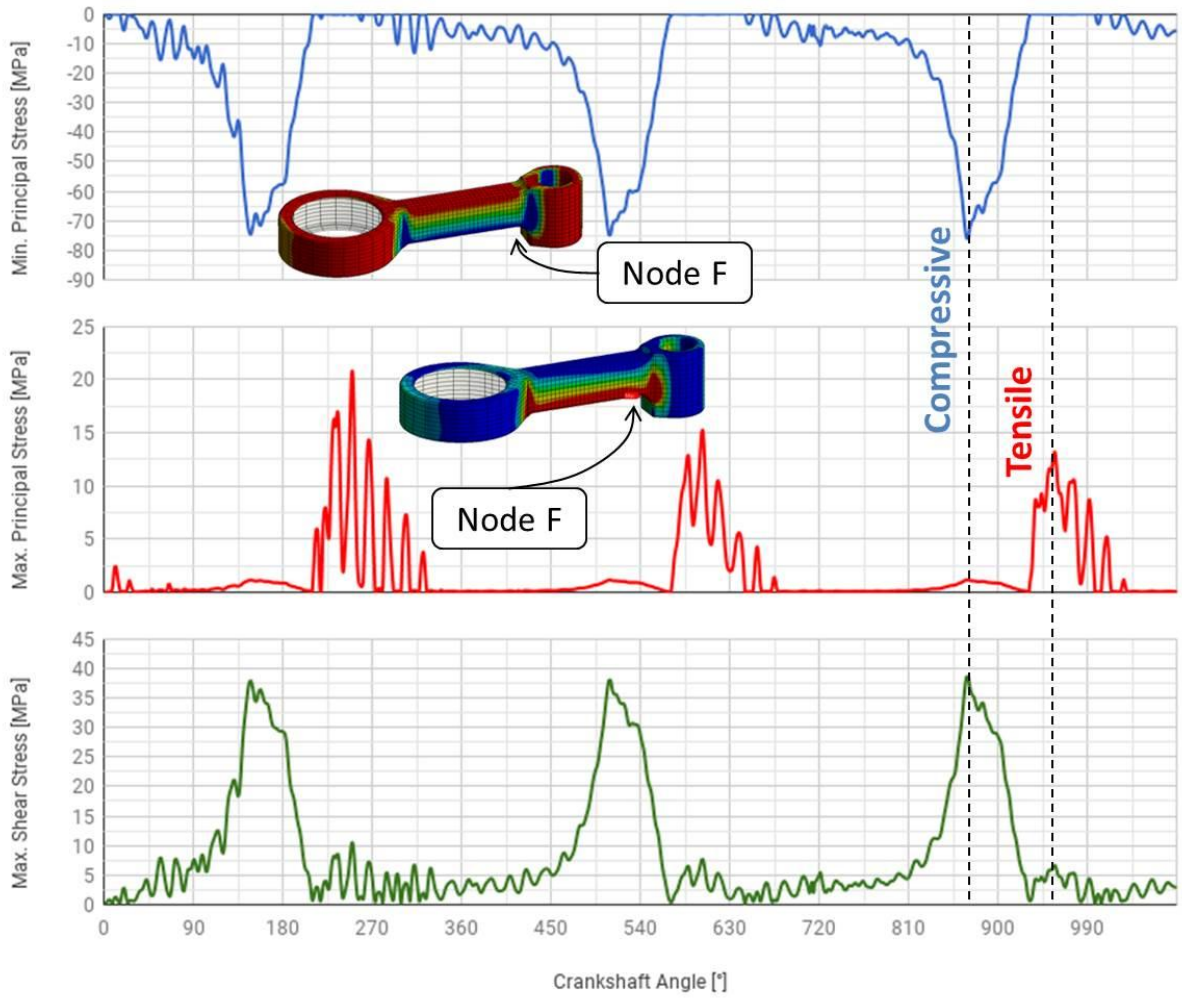

Source: Author's own figure, 2018.

Figure 24 - Principal Stresses for node H, located at lower right side of big end.

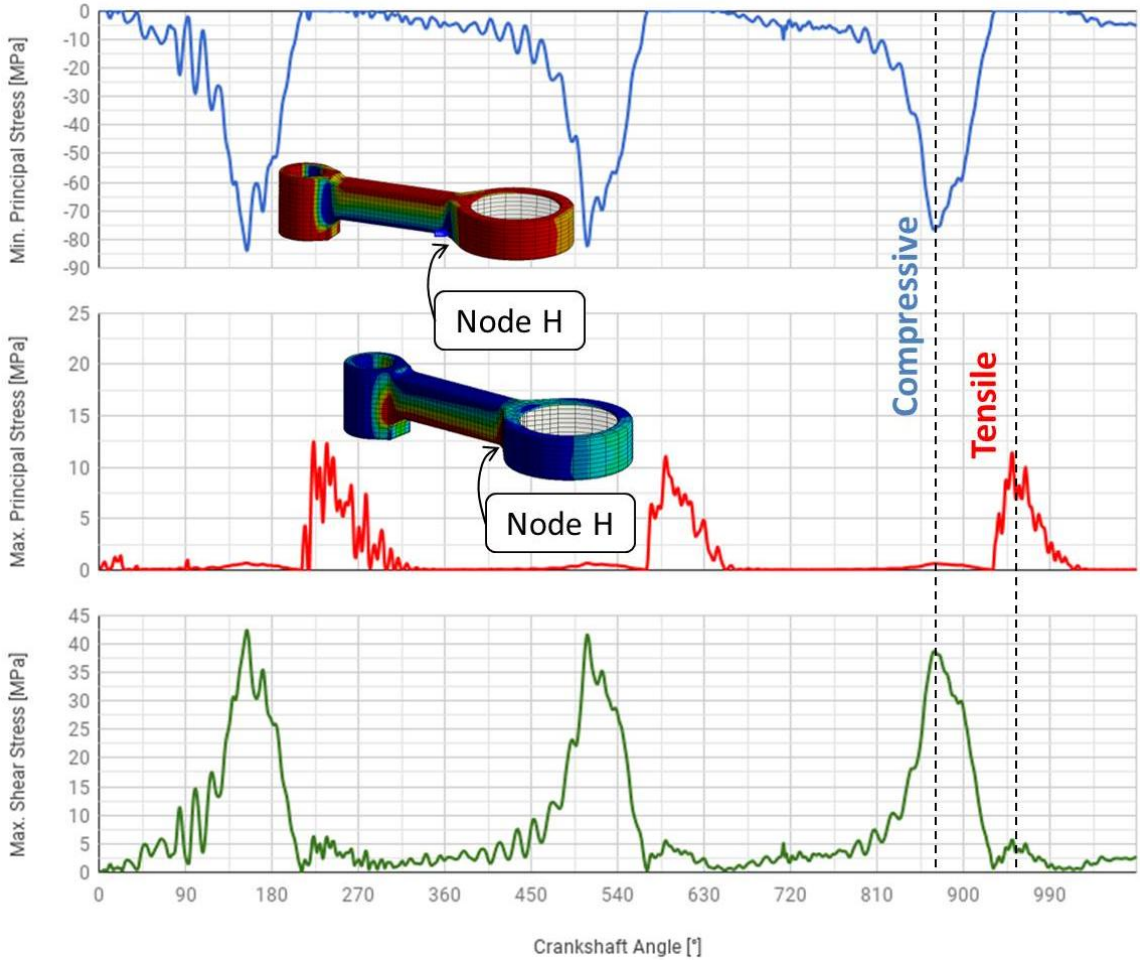

Source: Author's own figure, 2018.

For all evaluated nodes it is possible to notice that the stress profile during operation is similar to what happens to a standard specimen during uniaxial tensile-compressive fatigue bench test. Figure 25 shows a didactical example of Mohr circle of an element submitted to uniaxial stresses, compressive (a) and tensile (b).

Figure 25 - Mohr circle associated to tensile and compressive loads.

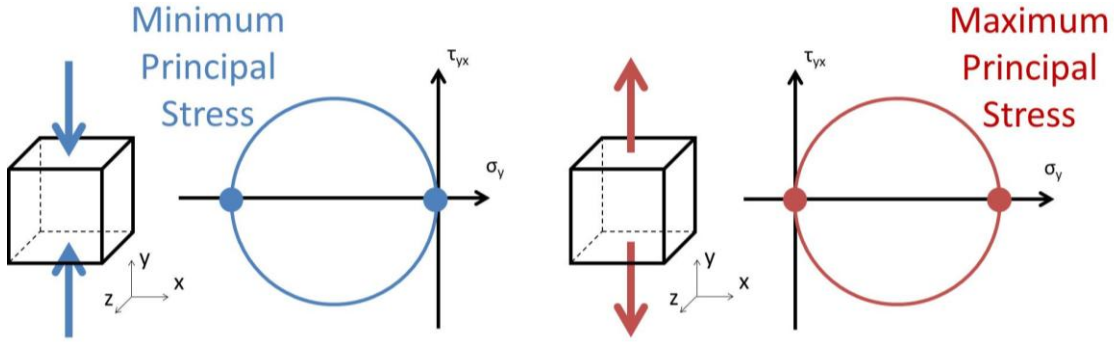

Source: Author's own figure, 2018.

During compression, close to Crankshaft angle 150°, Minimum Principal Stress reaches its maximum absolute value, while Maximum Principal Stress is zero and Maximum Shear Stress is half the Minimum Principal Stress. During tension, close to crankshaft angle 220°, Minimum Principal Stress is zero while Maximum Principal Stress reaches its maximum absolute value and Maximum Shear Stress is half the Maximum Principal Stress.

Although the connecting rod section is submitted to bending stresses, the critical nodes from Table 3 can be properly represented as uniaxial stress state. Therefore, the stress profile can be adjusted, simplified and treated as sinusoidal, as exemplified in Figure 26, in which blue dotted line represents node A, and red dashed line represents node E, black dot dash line represents node F and green solid line represents node H running in 1st main operating condition.

Figure 26 - Simplified sinusoidal stress profiles of connecting rod critical nodes.

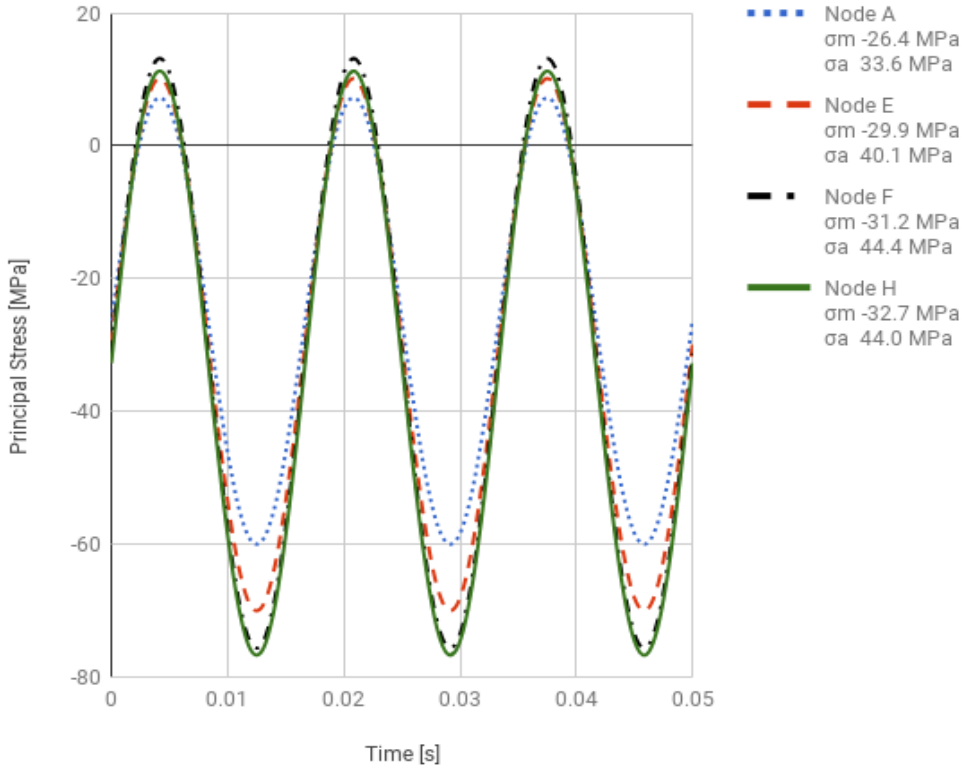

Source: Author's own figure, 2018.

Complete list of mean and alternating stress results for all evaluated nodes when the compressor is operating at the three main conditions are registered in Table 5.

Table 5 - Mean and Alternating stress for critical nodes running in main operation conditions.

	1st Main Condition		2nd Main Condition		3rd Main Condition	
Node	σm [MPa]	σa [MPa]	σm [MPa]	σa [MPa]	σm [MPa]	σa [MPa]
A	-26.4	33.6	-23.3	29.9	-18.2	25.4
B	-19.1	25.7	-16.9	23.4	-13.7	19.0
C	-27.1	33.9	-24.4	30.2	-19.4	25.2
D	-14.6	20.6	-13.1	18.0	-10.2	16.4
E	-29.9	40.1	-25.9	35.9	-19.0	31.3
F	**-31.2**	**44.4**	**-26.9**	**39.7**	**-21.6**	**32.9**
G	-20.0	26.9	-17.8	23.6	-12.3	20.8
H	-32.7	44.0	-29.2	39.2	-23.2	32.2

Source: Author's own table, 2018.

Table 5 results indicates that the range of mean stress that the connecting rod will be working during the compressor`s life is between -10.2 MPa and -42.8 MPa. This range is used to define the mean stress levels of the material S-N chart required to evaluate the component fatigue life. Furthermore, when the fatigue limit of the material for a given mean stress is known, this information can be used to calculate a fatigue safety factor or cycle counting, as discussed in future topics.

6.4 S-N CHART

Results from FEM numerical simulations in topic 6.3 show that, even that the connecting rod is also submitted to bending stresses close to section, the critical nodes stress profiles are equivalent to compression-tension tests. Hence, an exclusively axial dynamic test device is considered adequate to provide the required fatigue life information from the same standard specimen used for the quasi-static tests in topic 6.2.

Dynamic axial tests to characterize the relation between Alternating stresses and number of cycles to failure were done using a MTS 810 Material Test System for

axial tests, equipped with load cell with range up to 10 KN, 647 hydraulic wedge grip fixation pressure 1 Kpsi and operating oil flow 15 gallon per minute. MTS software TestStar^{TM} IIs Station Manager 4.0D applies a specific sine load profile to the samples and register number of cycles required to failure or survival.

Many compressor applications operate in single motor speed, 50Hz or 60Hz.There are applications with variable speed up to 75Hz, but it is not the focus of the present work. It is known that the test frequency has an important influence on the S-N fatigue curve results, so it is recommended to run the experimental tests in frequencies close to real component operation. Then, MTS dynamic axial tests are settled to run at 60Hz.

As mentioned previously, it is desirable to evaluate the fatigue behavior for the connecting rod material when submitted to compressive stresses in a range close to the real application. This range can be evaluated with minimum two fatigue curves with mean stress close to the application limits. Table 5 indicates that, considering all critical nodes in all operating conditions, the connecting rod is working under mean stresses from -10.2 MPa to -42.8 MPa, therefore two fatigue S-N curves, with mean stresses -50 MPa and 0 MPa, are enough to describe the application range.

Alternating stress levels are levels defined based on compressive Yield and ultimate strength from topic 6.2. Previous studies indicate that, for a zero mean stress situation, the fatigue limit (alternate stress) is usually between 20 and 30% of the ultimate tensile strength on static test. Considering that the material indeed has a fatigue limit, the Stress-Cycles curve characterization requires tests with alternate stress levels between 15% and 50% of the ultimate tensile strength.

Figures 27 (a) and (b) indicates the stress profiles (as function of time) applied to the standard specimen during the dynamic axial experimental evaluation to plot fatigue curves with mean stress -50 MPa and 0 MPa, respectively.

Figure 27 - Alternating stresses profile corresponding to -50 MPa and 0 MPa mean stresses.

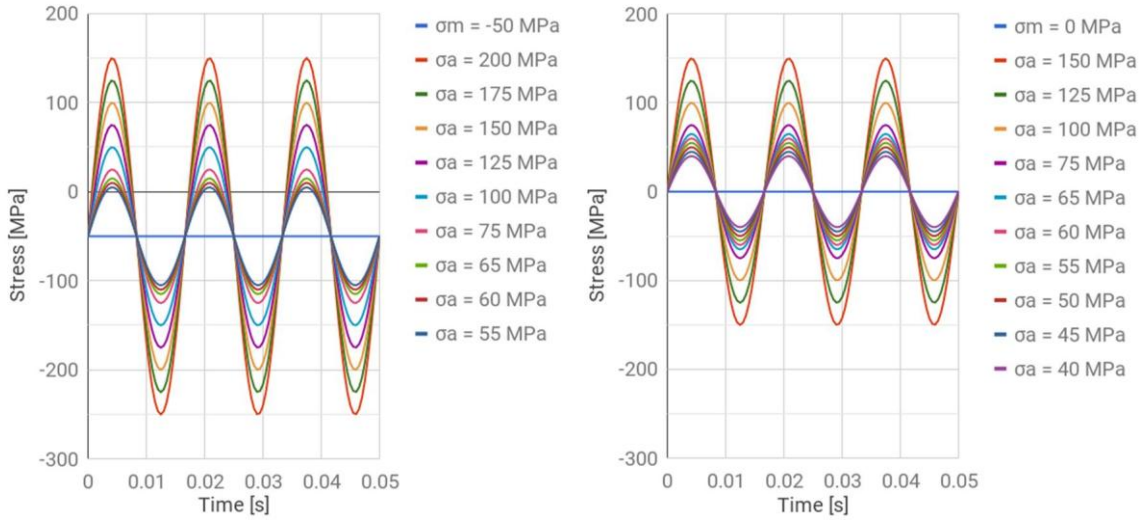

(a) (b)

Source: Author's own figure, 2018.

Each stress profile from Figure 27 is replicated minimum 3 times to generate points for the fatigue Stress-Cycles curve at the corresponding mean stress level. In case the standard specimen failure occurs out of interest region, the data is not considered and the test sequence is repeated. The S-N curve tendency is plotted using log scale in Figure 28. Tests are interrupted if the number of cycles to failure is too long and indicates a significant change on the curve trendline. Those cases are represented as "survival" and are not considered to calculate the curve trendline.

Figure 28 - Alternating Stress vs. Cycles to failure curves for -50 MPa and 0 MPa mean stresses.

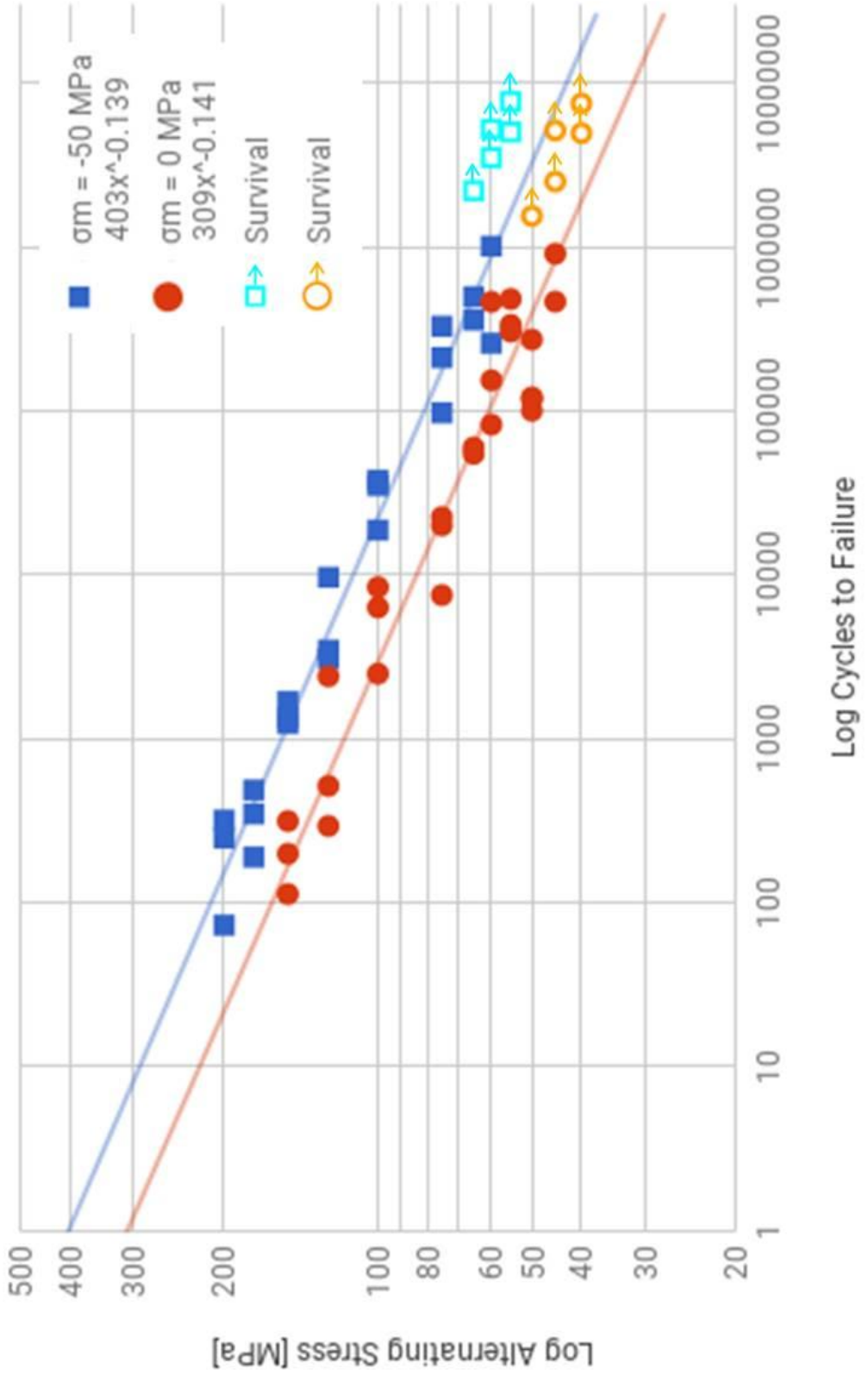

Source: Author's own figure, 2018.

Power series fit indicates the material fatigue behavior for each mean stress level, disregarding survival results. Representing the curves with the equation format $y = A * x^b$, Table 6 shows the Constant (A) and Exponential (b) coefficients for each mean stress level, demonstrating that the log-log S-N curves have a very similar inclination.

Table 6 - Power series fit coefficients describing fatigue trendlines.

σ_m [MPa]	A	b
-50	403	-0.139
0	309	-0.141

Source: Author's own production, 2018.

The interrupted tests confirm that there is a transition between High Cycle Fatigue and Very High Cycle Fatigue close to 10^6cycles. In accordance with the discussion inside literature review topic, trendline obtained with the failed samples clearly has an inclination change and the material fatigue behavior must be reevaluated to consider VHCF.

Many previous studies indicate that the transition between HCF and VHCF occurs with a slight decay inclination in the S-N curve. However, It was not feasible for the present work to run much more than 7.5e+6 cycles at 60Hz, so the Very High Cycle Fatigue and the HCF-VHCF transition can not be properly characterized. Therefore, the conventional fatigue limit concept is considered for the connecting rod evaluation and estimated based on a Staircase analysis with the failures and survival data previously indicated in Figure 28.

6.5 FAILURE ANALYSIS

Failed samples from S-N curve (topic 6.4) must be inspected to guarantee that the test properly reproduced the desired failure mode. The test validation basically consists on checking the failure location and possible presence of inclusions or defects that may have initiated the crack.

Material characterization through standard specimen is applicable for any component geometry, since it does not contain notch or stress concentrators and, thus, evaluates the material properties itself. Therefore, the standard specimen

failure must occur in a constant section region, as exemplified in Figures 29 and 30. Moreover, test stress level is calculated by the relation between the applied load and the standard specimen transversal area, so the region of interest must have the least deviation possible of width and thickness.

Figures 29 and 30 also indicates fracture angle in frontal view, lateral view and total fracture plane angle (bottom of figure). Fracture angles of all samples were measured, but not registered since it is not the main focus of the present work.

Figure 29 - Failure location checking for Mean stress -50 MPa and Alternating Stress 175 MPa (a), 125 MPa (b) and 65 MPa (c).

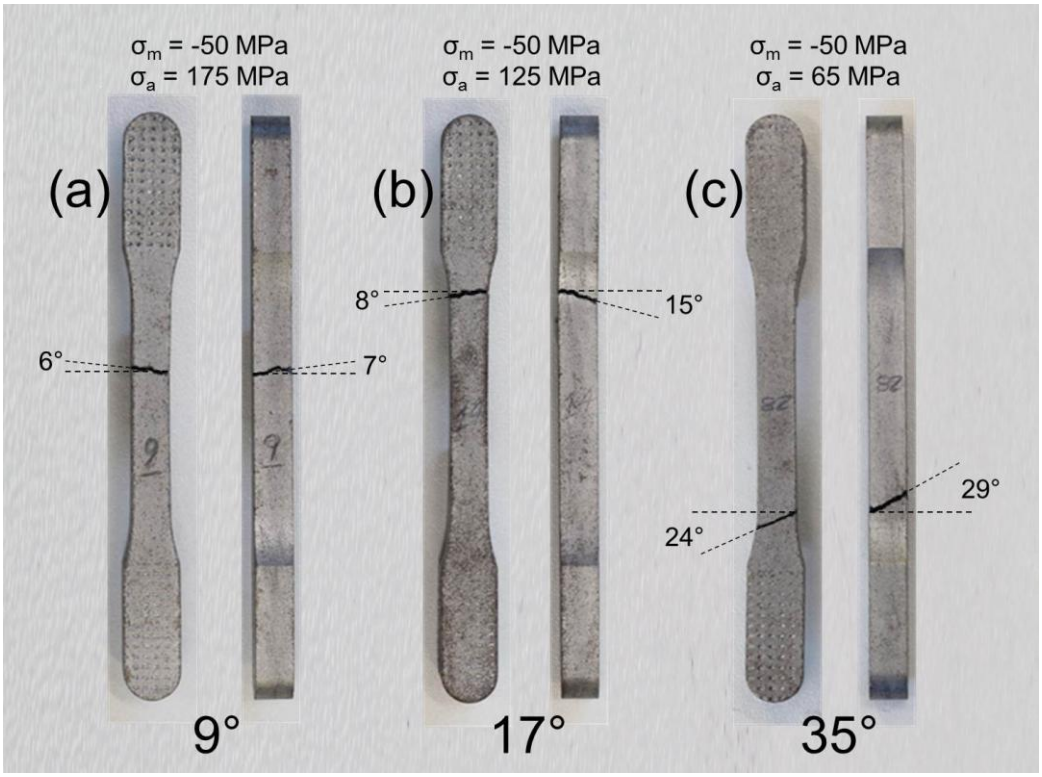

Source: Author's own figure, 2018.

Figure 30 - Failure location checking for zero Mean stress and Alternating Stress 100 MPa (a), 75 MPa (b) and 50 MPa (c).

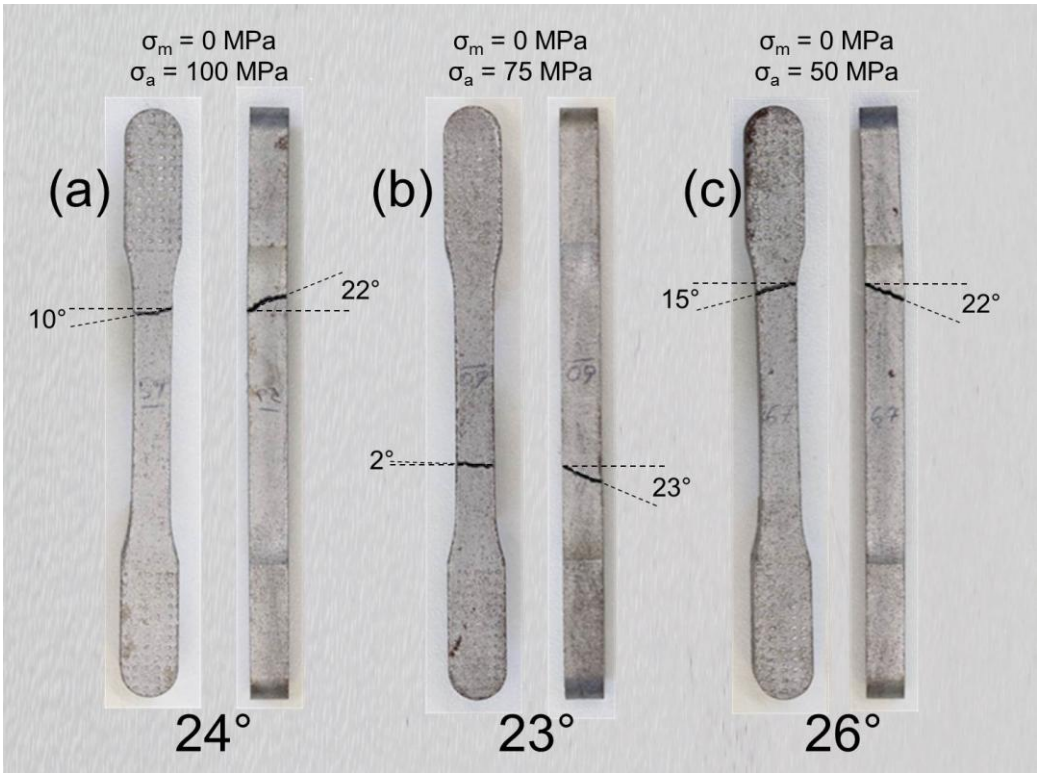

Source: Author's own figure, 2018.

Validation was done for all failures from S-N curves in topic 6.4 Examples from Figure 29 (a), (b) and (c) show that, for compressive mean stresses, there is a tendency of increasing fracture angle for lower alternating stresses (angles from 9° to 35°). The fracture angle is caused by the shear stress existent out of principal planes, as shown in Mohr circle from Figure 25. On the other hand, Figure 30 (a), (b), and (c) show that the fracture also occurs in an inclined plane (around 25°), but the angle increasing tendency was not observed.

Additionally, the presence of inclusions or defects that may have initiated the crack must be checked. Figures 31 and 32 exemplify the failures visual analysis with optical microscope. Correspondent operating load and fracture angle are also registered for each figure (a), (b) and (c).

Figure 31 - Internal defect evaluation for Mean stress -50 MPa and Alternating Stress 175 MPa (a), 125 MPa (b) and 65 MPa (c).

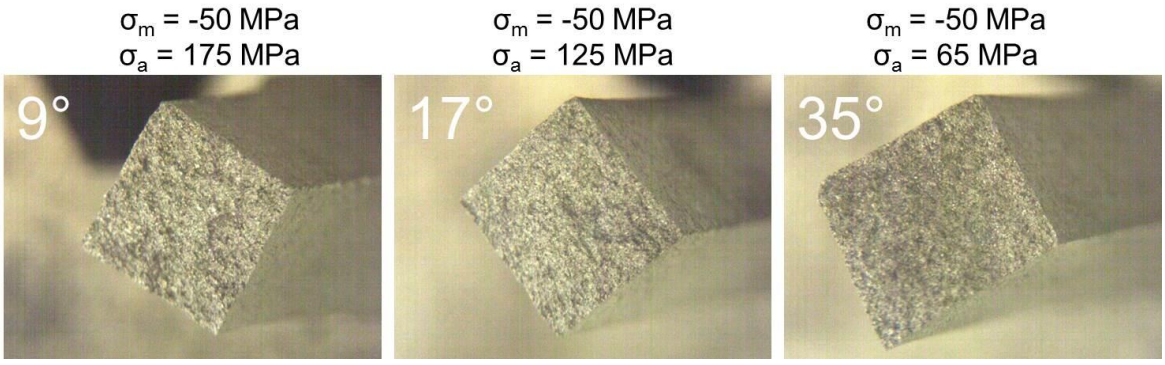

(a) (b) (c)

Source: Author's own figure, 2018.

Figure 32 - Internal defect evaluation for zero Mean stress and Alternating Stress 100 MPa (a), 75 MPa (b) and 50 MPa (c).

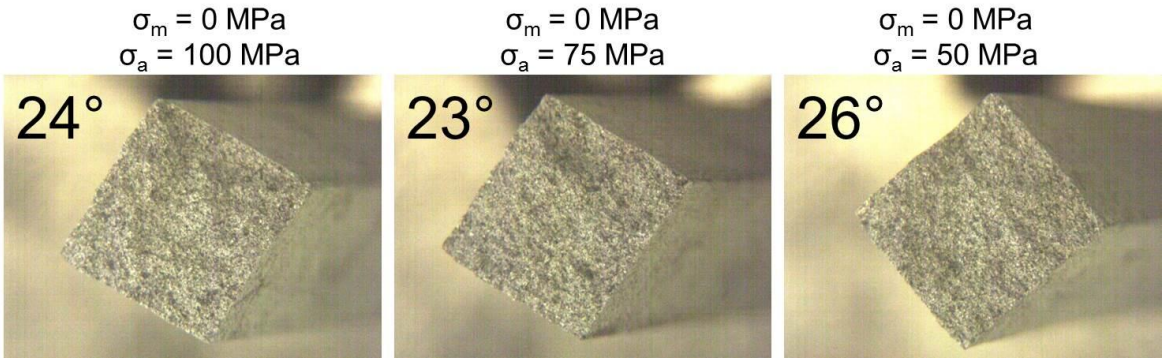

(a) (b) (c)

Source: Author's own figure, 2018.

Failure analysis was done for all tested samples, and no evidences of inclusions or defects were observed, confirming that the experimental data obtained during dynamic experimental tests can be prudently used to describe the fatigue behavior of the sintered material.

6.6 CONVENTIONAL FATIGUE LIMIT

The staircase method is able to calculate the material fatigue limit for a specific number of cycles using statistical treatments of the data obtained in topic 6.4. From JSME S 002 standard, the methodology depends on a rough initial estimation of the material fatigue limit, slightly above the stress level of a suspended test, and

indicates the alternating stress to submit the next standard specimen based on the previous evaluation.

If failure occurs before completion of stipulated number of cycles, the next specimen is tested at one step stress (d) lower. If the test reaches the required number of cycles, the test is interrupted and the next specimen is tested at higher stress level, always keeping the same stress step between runs.

The Dixon-mood method provides equations to calculate the average and standard deviation of the material fatigue limit by using the data of less frequent event out of the two possible events i.e. survivals or failures.

If “survival” is the less frequent event, the average fatigue limit is given by Equation 2.

$$\mu_S = S_0 + d * \left(\frac{A_{DM}}{\sum n_{DM,i}} + \frac{1}{2}\right) \quad (2)$$

Where $A_{DM} = \sum(i) * (n_{DM,i})$ and $n_{DM,i}$ is the count of less frequent event corresponding to the i^{th} stress amplitude and S_0 is the lowest stress amplitude ($i = 0$).

The standard deviation is estimated from Equation 3.

$$\sigma_S = 1.62 * d * \left[\frac{B_{DM} * \sum n_{DM,i} - {A_{DM}}^2}{(\sum n_{DM,i})^2} + 0.029\right] \quad (3)$$

Where $B_{DM} = \sum(i^2) * (n_{DM,i})$.

Figure 33 describes the outcome of dynamic axial tests to apply the staircase method at compressive mean stress -50 MPa.

Figure 33 - Staircase method to define fatigue limit associated to -50 MPa mean stress.

	σm = -50 MPa		
#	σa [MPa]	Cycles	Outcome
1	65.0	358100	Failure
2	60.0	258306	Failure
3	55.0	5021411	Survival
4	60.0	5224077	Survival
5	65.0	495499	Failure
6	60.0	1008043	Failure
7	55.0	7720125	Survival
8	60.0	3504361	Survival
9	65.0	2000000	Survival

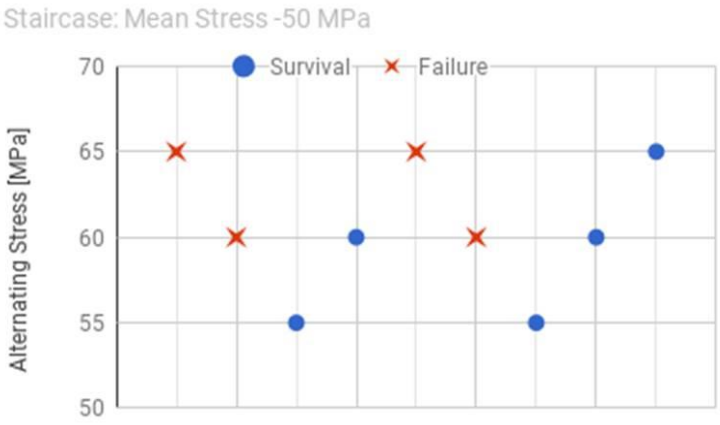

Source: Author's own figure, 2018.

Dixon-mood equations calculate average fatigue limit 60 MPa and standard deviation 2.65 MPa for 3.5e+6 cycles. In the absence of enough data to actually estimate the distribution shape, it is conservatively recommended to treat it as a normal distribution and subtract 3 standard deviations from the average to define the statistical fatigue limit of the material. Hence, for compressive mean stress -50 MPa, the lower bound of the endurance limit is considered as 52.05 MPa.

Figure 34 describes the outcome of dynamic axial tests to apply the staircase method at zero compressive mean.

Figure 34 - Staircase method to define fatigue limit associated to 0 MPa mean stress.

	σm = 0 MPa		
#	σa [MPa]	Cycles	Outcome
1	55.0	481291	Failure
2	50.0	100289	Failure
3	45.0	907887	Failure
4	40.0	4938687	Survival
5	45.0	2503230	Survival
6	50.0	118169	Failure
7	45.0	463797	Failure
8	40.0	7000005	Survival
9	45.0	5127645	Survival

Source: Author's own figure, 2018.

Dixon-mood equations calculate average fatigue limit 45 MPa and standard deviation 2.65 MPa for 2.5e+6 cycles. In the absence of enough data to actually estimate the distribution shape, it is conservatively recommended to treat it as a

normal distribution and subtract 3 standard deviations from the average to define the statistical fatigue limit of the material. Hence, for zero mean stress, the lower bound of the endurance limit is considered as 37.05 MPa.

In compliance with lower bounds of statistical distributions, the inferior limit of the fatigue curve for finite life region (HCF) must be considered likewise. It is important for cycle counting in case when alternating stress during operation are higher than the material endurance limit. Software Reliasoft ALTA is used to plot the confidence interval of fatigue curves from figure 28. It considers both failure and survival tests and is described as Weibull Inverse Power Law distribution defined by β, K and n parameters. Figures 35 and 36 show the 99.73% confidence interval for fatigue curves with -50 MPa mean stress (β = 1.451, K = 4.688e-22 and n = 8.330) and zero mean stress (β = 1.155, K = 5.441e-20 and n = 7.794), respectively.

Figure 35 - Confidence interval of S-N curve associated to mean stress -50 MPa.

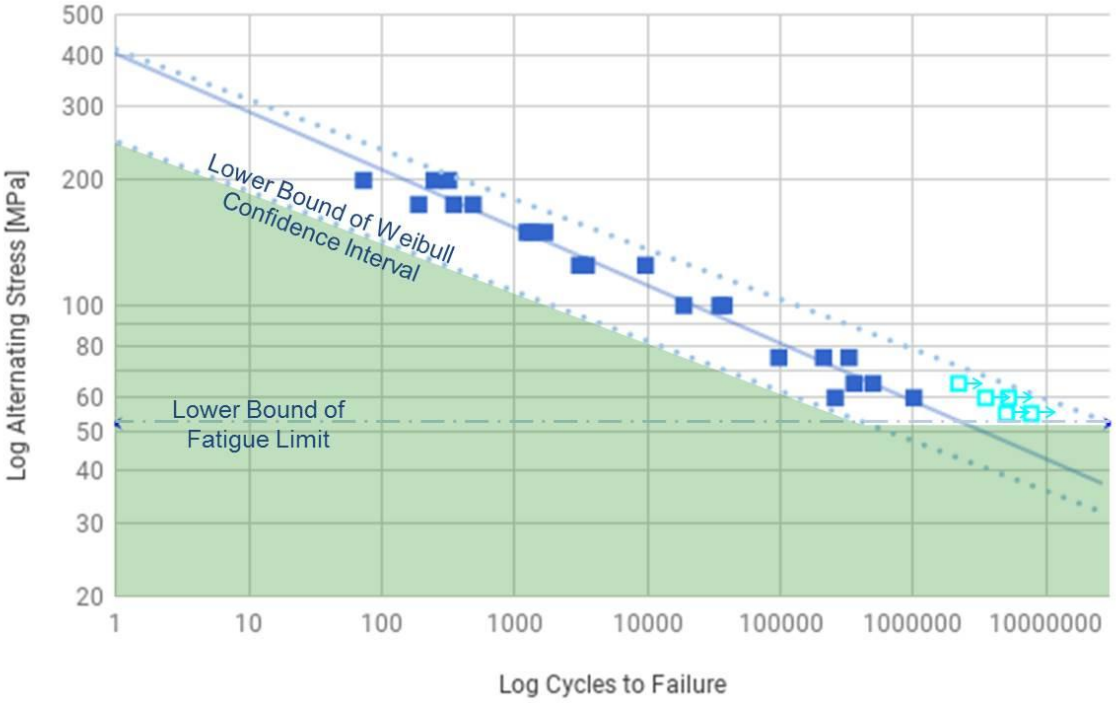

Source: Author's own figure, 2018.

Figure 36 - Confidence interval of S-N curve associated to mean stress 0 MPa.

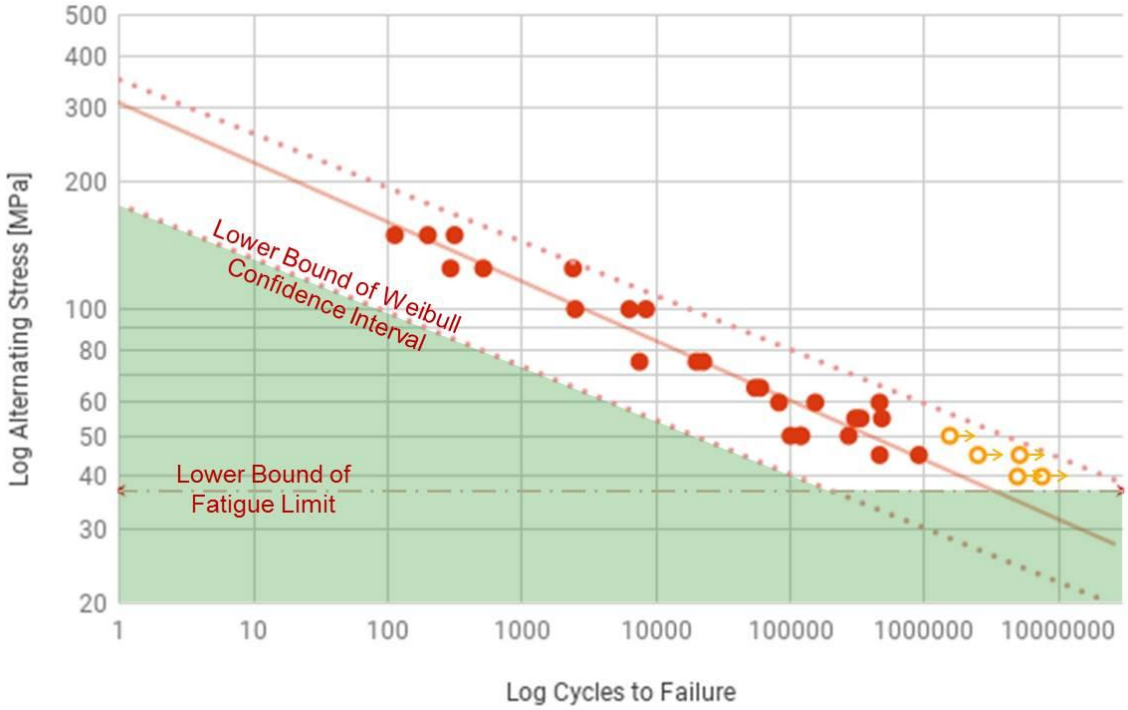

Source: Author's own figure, 2018.

It can be noticed that, for the sintered material under evaluation, the average of conventional fatigue limit is equivalent to 40% of the average tensile Yield strength and approximately 25% of the average ultimate tensile strength for a zero mean stress situation.

6.7 FATIGUE CRITERIA

Classic literature from Lee et al. (2005) mentions that empirical models by Gerber (1874), Goodman (1899), Haigh (1917), and Soderberg (1930) were proposed to compensate for the tensile normal mean stress effects on high-cycle fatigue strength. These empirical models can be plotted as constant life diagrams, most commonly alternating stress (σa) versus mean stress (σm).

Disregarding statistical standard deviations, the fatigue limit estimated from two S-N curves generates two points in the σa versus σm diagram. Therefore, a straight line linking the two points gives a simplified idea of the alternating fatigue limit for any mean stress level inside the evaluated range.

Figure 37 shows the constant life diagram containing both material fatigue limits (average values) obtained through the Staircase method, connected by the thick continuous blue line. An extension of Goodman and Soderberg criterions are plotted as dotted red and green lines, for comparison purposes.

Figure 37 - Constant life diagram.

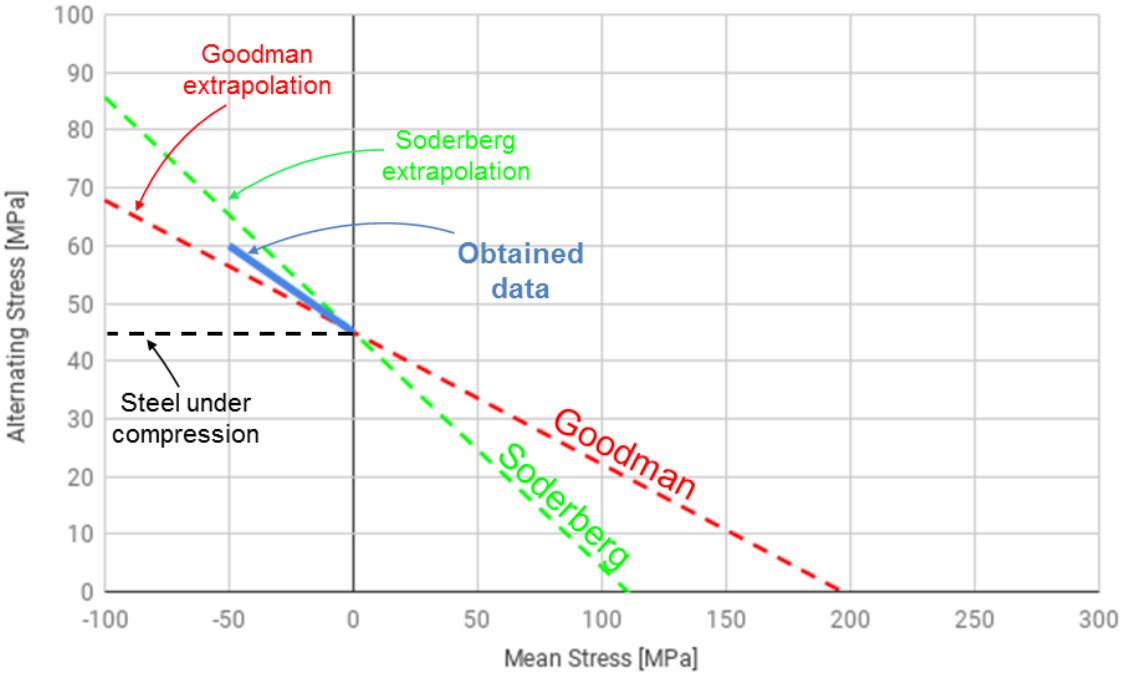

Source: Author's own figure, 2018.

The obtained experimental data seems to be intermediate between classic Soderberg and Goodman criterias when submitted to compressive mean stresses. Extending the linear behavior of the experimental fit, a mean stress compensation factor (MSCF) is used to convert any alternating stress value to an Modified Alternating Stress, as if was tested at zero mean stress, through the Equation 4.

$$\sigma_{a_{mod}} = \frac{\sigma_a}{\left(\frac{1}{\sigma_m / MSCF}\right)} \tag{4}$$

If MSCF tends to infinite, no compensation is applied. For an optimum MSCF value, data from different mean stress levels should equivalently overlap and the coefficient of determination R^2 of the full data should be maximum, indicating a

logarithmic tendency. Excluding survival data, figure 38 shows the variation of coefficient of determination R^2 as a function of the MSCF value.

Figure 38 - Mean Stress Compensation factor determination.

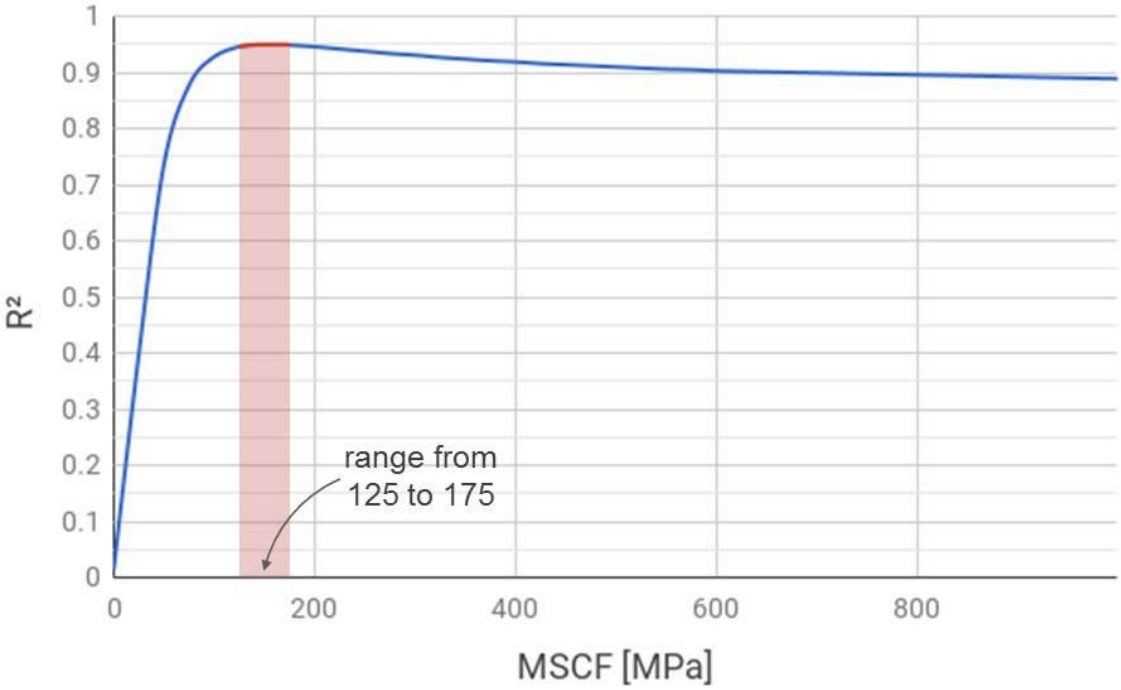

Source: Author's own figure, 2018.

MSCF values from 125 MPa to 175 MPa correspond to maximum R^2 possible 0.95. Therefore, applying MSCF range median value to Equation 4, modified alternating stress for both fatigue curves are overlap inside the same trendline, as shown in figure 39.

Figure 39 - Mean Stress Compensation factor validation.

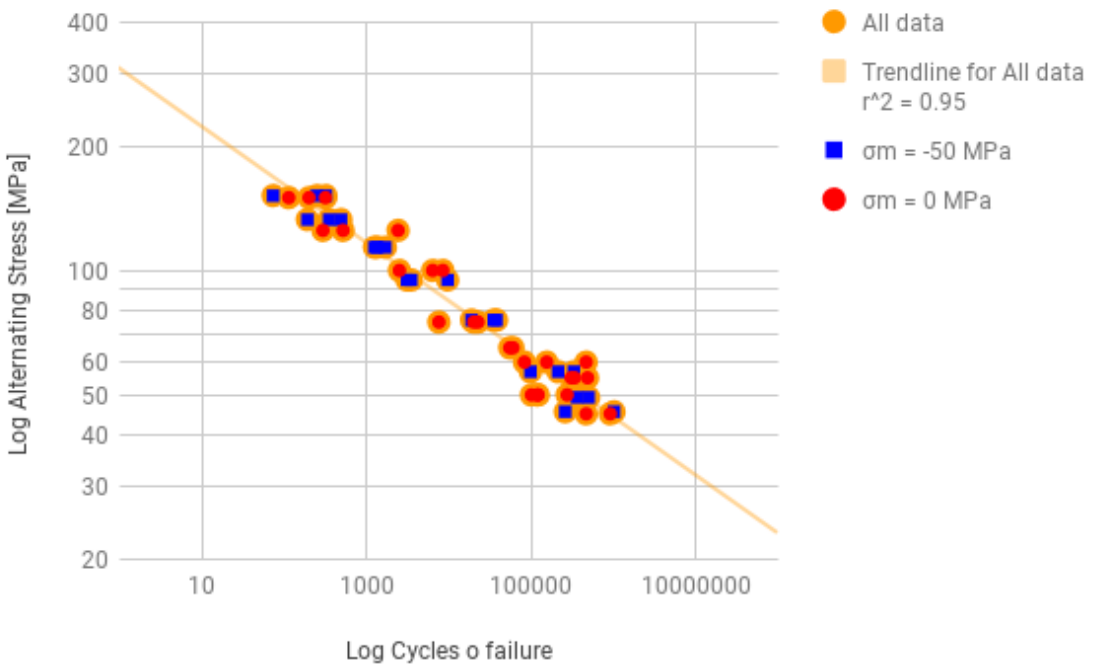

Source: Author's own figure, 2018.

It can be noticed that the mean value of MSCF (150 MPa) is 35% higher than the material's Yield strength, measured in topic 6.2. Therefore, this relation can be used to adjust the Soderberg criteria and to predict the endurance limit corresponding several mean stress levels in which the connecting rod works, as described in numerical simulations topic 6.3.

6.8 FATIGUE SAFETY FACTOR:

Being aware that the Mean Stress Compensation Factor is 35% higher than the material Yield strength, and the adjusted Soderberg criteria is valid for mean stress levels between 0 MPa and -50 MPa, it is possible to convert an alternating stress value at any given mean stress level to an equivalent alternating stress associated to a different mean stress level. Therefore, the Adjusted Soderberg criteria allows a conjecture about the fatigue limit for any mean stress level within the evaluated range.

However, average values are not enough to ensure reliability of mass production batches. Statistical deviations must be considered to guarantee that the product can withstand operating loads even when produced close to design

specification limits. Assuming a conservative approach to calculate the fatigue safety factor from the constant life diagram, Yield strength values (topic 2) and fatigue limit data (topic 5) are treated as normal distributions. Hence, 99.73% of the Probability Density Function is equivalent to 3 standard deviations of each distribution.

Accordingly, sintered material Yield strength should vary between 95 and 128 MPa, while fatigue limit with mean stress -50 MPa should vary between 52 and 68 MPa, and fatigue limit with mean stress 0 MPa should vary between 37 and 53 MPa. Figure 40 shows the constant life diagram indicating the lower bound of the Adjusted Soderberg criteria to be used on the safety factor calculation.

Figure 40 - Adjusted Soderberg fatigue criteria.

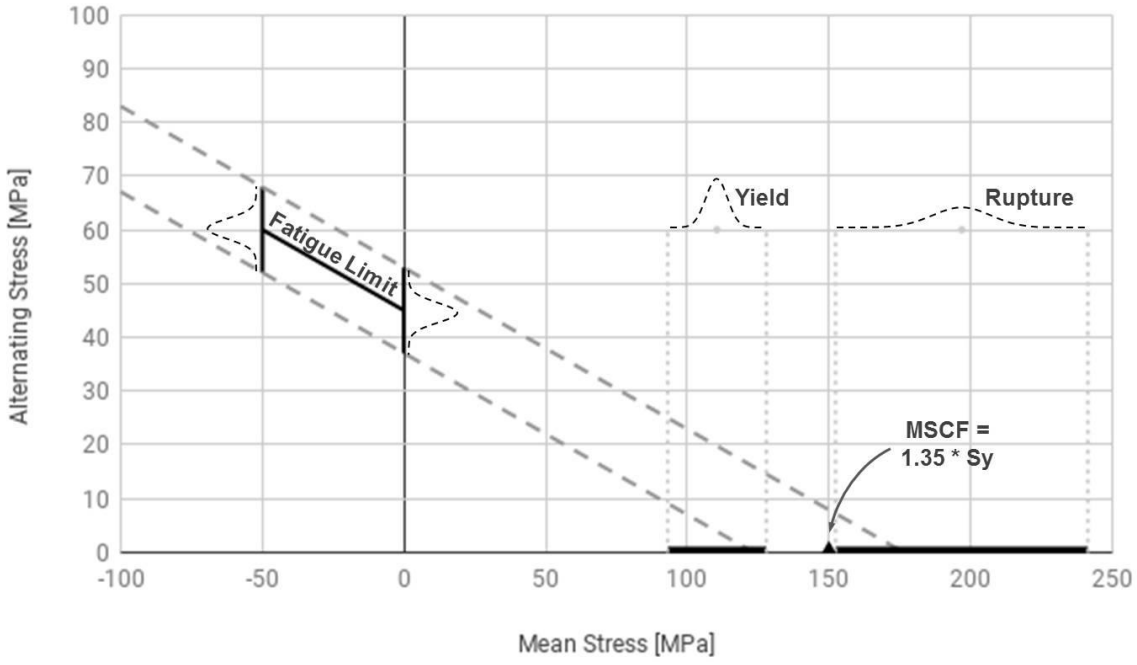

Source: Author's own figure, 2018.

As described in topic 6.7, it is possible to convert any alternating stress value to a modified alternating stress, as if tested at zero mean stress, through Equation 4. Following the Adjusted Soderberg criteria, the fatigue safety factor at any connecting rod node, running within the evaluated mean stress range, is calculated through the Equation 5.

$$S_f = \frac{Se}{\left(\frac{\sigma_a}{1-{\sigma m}/{1.35*Sy}}\right)} \quad (5)$$

In which the Yield strength Sy is conservatively equivalent to the lower limit of the normal distribution for the material Yield strength, 95 MPa.

From numerical simulations in topic 6.3, Tables 7, 8 and 9 contain Alternating (σ_a) and Mean (σ_m) stresses information for connecting rod nodes A to H (described in Table 3) when the compressor is running at main operating conditions (described in Figure 8). The associated safety factor (S_f) for each node at each condition is used to understand if the component is reliable enough to transcend the number of cycles in which the fatigue S-N curve reaches the conventional fatigue limit.

Table 7 - Connecting rod critical nodes safety factor running at 1st main operating condition.

1st Main Operating Condition				
Node	σ_m [MPa]	σ_a [MPa]	$\sigma_{a_{mod}}$ [MPa]	S_f
A	-26.4	33.6	27.8	1.33
B	-19.1	25.7	22.3	1.66
C	-27.1	33.9	27.9	1.33
D	-14.6	20.6	18.5	2.00
E	-29.9	40.1	32.4	1.14
F	**-31.2**	**44.4**	35.6	1.04
G	-20.0	26.9	23.2	1.60
H	-32.7	44.0	35.0	1.06

Source: Author's own production, 2018.

Table 8 - Connecting rod critical nodes safety factor running at 2nd main operating condition.

2nd Main Operating Condition				
Node	σ_m [MPa]	σ_a [MPa]	$\sigma_{a_{eq}}$ [MPa]	S_f
A	-23.3	29.9	25.3	1.47
B	-16.9	23.4	20.7	1.79
C	-24.4	30.2	25.3	1.47
D	-13.1	18.0	16.3	2.27
E	-25.9	35.9	29.8	1.24
F	**-26.9**	**39.7**	32.7	1.13
G	-17.8	23.6	20.6	1.80
H	-29.2	39.2	31.8	1.16

Source: Author's own production, 2018.

Table 9 - Connecting rod critical nodes safety factor running at 3rd main operating condition.

3rd Main Operating Condition				
Node	σ_m [MPa]	σ_a [MPa]	$\sigma_{a_{eq}}$ [MPa]	S_f
A	-18.2	25.4	22.2	1.67
B	-13.7	19.0	17.1	2.16
C	-19.4	25.2	21.9	1.70
D	-10.2	16.4	15.2	2.44
E	-19.0	31.3	27.2	1.36
F	**-21.6**	**32.9**	28.1	1.32
G	-12.3	20.8	19.0	1.95
H	-23.2	32.2	27.2	1.36

Source: Author's own production, 2018.

Fatigue limit for connecting rod Mean stress range running at main operating conditions was purposely characterized. Yet, the material behavior for different mean stress levels can be conservatively estimated for distinct applications. Figure 41 suggests a conservatory estimation for a Yield and Fatigue safety envelope (green

area), based on the static and dynamic experimental evaluations done during the connecting rod material characterization.

Figure 41 - Yield and fatigue safety envelope.

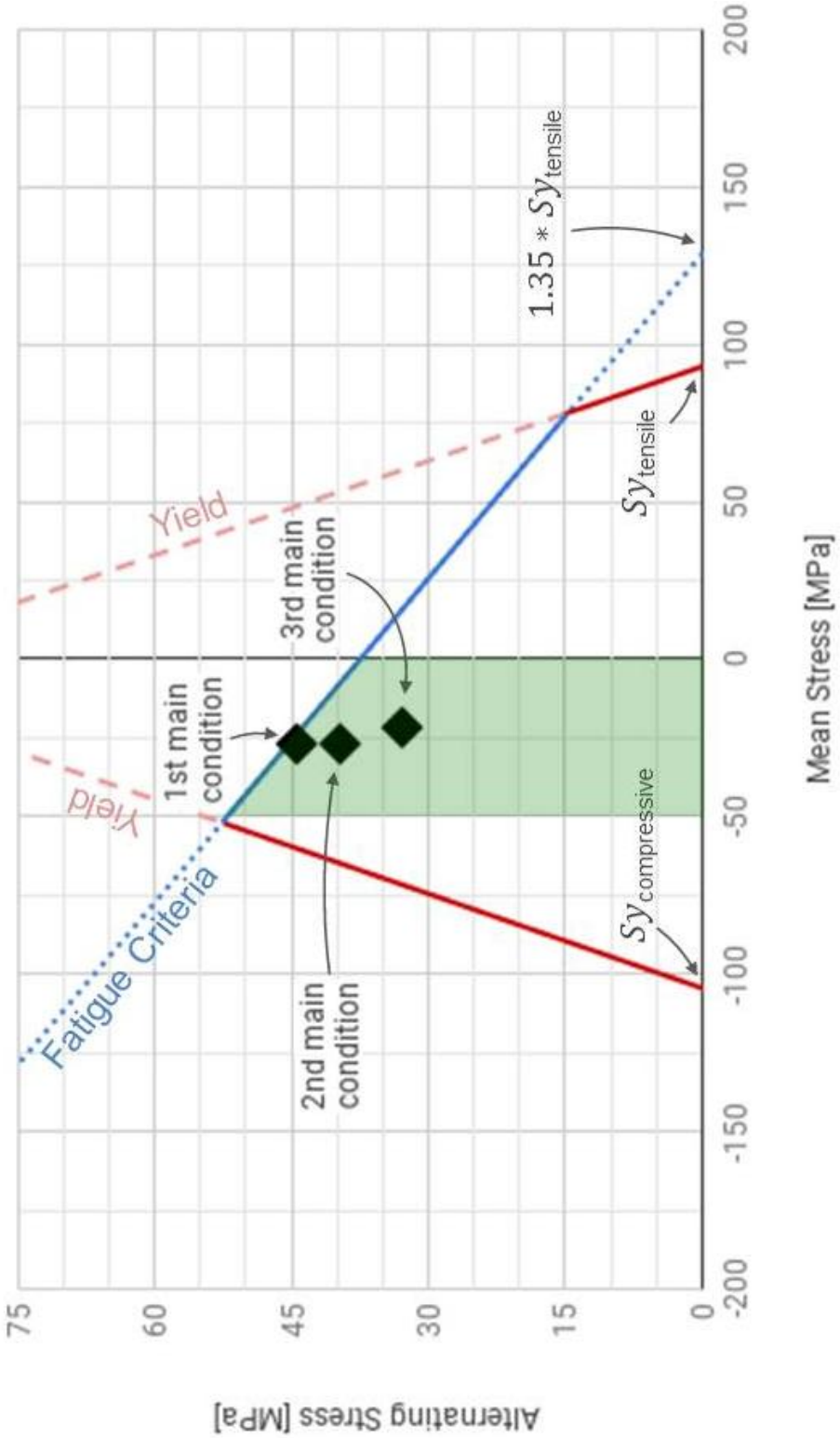

Source: Author's own figure, 2018.

Mean stress range from -50MPa to 0 MPa was characterized in topic 6.6. Assuming that the fatigue behavior is kept for positive mean stress levels, the blue continuous line describes the material fatigue behavior for mean stresses from -50 MPa to approximately 75 MPa, where the application is limited by the tensile Yield stress red dashed line.

The tendency of the material fatigue behavior, for compressive mean stresses lower than -50 MPa, is to increase up to an undetermined point and, eventually decrease until static compression rupture. Nonetheless, at mean stress slightly below -50 MPa the application is limited by the compressive Yield stress red dashed line.

Lastly, figure 41 yet indicates σ_a and σ_m for critical node F when the connecting rod is running at the 3 main operating conditions, represented as black solid diamonds.

7 CONCLUSIONS

The proposed methodology to evaluate the connecting rod fatigue safety factor is based on reciprocating compressor operating conditions summarization, material characterization, numerical simulations to evaluate operating stresses, dynamic uniaxial bench tests with standard specimen to determine the material fatigue limit and definition of a fatigue criteria compliant with the evaluated material.

Material characterization with standard specimen is important for comparison with similar alloys. The evaluated sinter material, with basic composition Fe + 0.5%Si + 4%Ni +6.5%vo. C +1%vol. hBN + 0.8% Lube-E and compact density 6300 ± 235 Kg/m³, has Young Modulus, at both compressive and tensile behavior, equivalent to 99 ± 12 GPa. Average Yield strength is also similar for tensile and compressive loads, 110 MPa and 135 MPa, respectively. However, as expected, there is a significant difference regarding ultimate strength and maximum elongation. For tensile loads, material rupture occurs at average stress 197 MPa and elongation 0.6%, while for compressive loads rupture occurs at average stress 328 MPa and elongation 2%.

Comparing material Yield strength and real compressor loads, it is concluded that a linear elastic FEM transient structural simulation is adequate to represent the connecting rod stress levels during operation. Furthermore, mapped hexahedral mesh with quadratic element size 1mm and timestep 7.04e-05s achieves good results convergence with feasible computational cost.

Monitoring critical node stress results during one complete cycle, it is noticed a satisfactory analogy between connecting rod real application and uniaxial bench tests with standard specimen. Hence, mean stress application range obtained from transient structural numerical simulations is used to define the dynamic experimental tests load levels to characterize the material fatigue behavior.

Evaluation of two fatigue S-N curves indicates parallel power law trendlines for zero and -50 MPa mean stress levels. Around 10^6 cycles, test data deviates from trendline, indicating inclination change which characterizes a transition between HCF and VHCF. The present work adopts the conventional fatigue limit concept, instead of VHCF second S-N inclination after the transition step. As described in literature review topic, High Cycle Fatigue regime, with internal crack initiation, is usually observed after 10^8 cycles, and it was not feasible to carry out so long evaluations

running at 60 Hz. Accelerated tests were not considered because S-N curve at higher frequencies might not be representative.

Hence, tests are suspended when the number of cycles to failure transcends the trendline confidence interval and the suspension data is used to estimate the conventional fatigue limit through the Staircase method. With 9 subsequent tests for each S-N curve, the conventional fatigue limit for zero mean stress level is calculated as 45 ± 8 MPa, while conventional fatigue limit for -50 MPa mean stress level is calculated as 60 ± 8 MPa. It confirms the benefit of compressive mean stress levels to the material fatigue limit.

Main conclusion is that the fatigue behavior of the evaluated sintered material under compressive mean stress can be properly described by a fatigue criteria intermediate between classical Soderberg and Goodman. Statistical correlation between two S-N trendlines demonstrates that the Mean Stress Compensation Factor is 35% higher than the material average Yield strength, and the Adjusted Soderberg criteria has satisfactory compliance with the obtained experimental data. Therefore, the average conventional fatigue limit, for zero mean stress, is equivalent to 40% of the average tensile Yield strength and approximately 25% of the average ultimate tensile strength.

The connecting rod minimum safety factor within the compressor operation envelope is 1.04. It is considered too low for mass production because numerical simulations were run applying average Young Modulus and geometrical deviations were not taken into account. Furthermore, compressor in real applications might run out of its operating envelope, and higher condensing temperatures may cause the connecting rod stresses to exceed the material fatigue limit, with consequent compressor field failure.

However, the proposed methodology does not consider the very low notch sensitivity of the sintered material, and the numerical results of stress are overestimated. Hence, the evaluated material has great potential to be applied in refrigeration compressors, conditioned to satisfactory tribological results.

8 SUGGESTIONS FOR FUTURE WORKS

- Evaluate S-N fatigue curves with tensile mean stress;
- Run longer duration experimental bench tests to evaluate failures in VHCF;
- Evaluate numerical results disregarding sintered material notch sensitivity;
- Investigate correlation between dynamic loads and with fracture angle;

9 REFERENCES

ANUSHA, B.; Reddy, C.vijaya Bhaskar. **Modeling and Analysis of Two Wheeler Connecting Rod by Using Ansys**. IOSR Journal of Mechanical and Civil Engineering (IOSR-JMCE) e-ISSN: 2278-1684,p-ISSN: 2320-334X, Volume 6, Issue 5 (May. - Jun. 2013), PP 83-87;

AZEEZ, Abass Adeyinka. **Fatigue Failure and Testing Methods**. Bachelor's thesis, HAMK University of Applied Science, 2013;

BINDER, Roberto. **Influência do Processo de Ferroxidação nas Propriedades de Ferro Sinterizado**. Universidade Federal de Santa Catarina. Curso de Pós-Graduação em Engenharia e Ciência dos Materiais, 1996;

DANNINGER, Herbert; Weiss, Brigitte. High Cycle Fatigue Of Powder Metallurgy Materials. VIII Congreso Nacional de Propiedades Mecánicas de Sólidos. Gandia, p. 195-204. oct. 2002;

GODEŽ, Srečko; Šori, Marko; Verlak, Tomaž. A Computational Model for Bending Fatigue Analyses of Sintered Gears. Strojniški vestnik - Journal of Mechanical Engineering, [S.l.], v. 60, n. 10, p. 649-655, oct. 2014. ISSN 0039-2480;

GOSNEY, W.B., Principles of Refrigeration, Cambridge, England: Cambridge University Press, 1982, 666 p;

G. T. BROWN & J. A. Steed (1973) The Fatigue Performance Of Some COnnecting Rods Made By Powder Forging, Powder Metallurgy, 16:32, 405-415, DOI: 10.1179/pom.1973.16.32.015;

J. M. WHEATLEY & G. C. Smith (1963) The Fatigue Strength Of Sintered Iron Compacts, Powder Metallurgy, 6:12, 141-158, DOI: 10.1179/pom.1963.6.12.011;

KAZYMYROVYCH, Vitaliy. Very High Cycle Fatigue of Engineering Materials, A Literature Review. Faculty of Technology and Science Materials Engineering, 2009;

LEE, Yung-li et al. Fatigue Testing and Analysis: Theory and Practice. Burlington: Elsevier, 2005. 417 p;

PEDROSO, Altemir Palmede. Desenvolvimento De Um Sistema Especialista Protótipo Para Suporte Ao Diagnóstico De Problemas De Baixo Desempenho De Compressores Herméticos. 2013. 151 f. Dissertação (Mestrado) - Curso de Engenharia Mecânica, Universidade Federal de Santa Catarina, Florianópolis, 2013;

POLASIK, S. J., Williams, J. J., Chawla, N., & Narasimhan, K. S. (2001). Fatigue crack initiation and propagation in ferrous powder metallurgy alloys. In Advances in Powder Metallurgy and Particulate Materials. (pp. 2042-2056);

POLASIK, S.J., Williams, J.J. & Chawla, N. Metall and Mat Trans A (2002) 33: 73. doi:10.1007/s11661-002-0006-8;

PUFF, Rinaldo. Estudo de fadiga para materiais ferrosos com vazios e inclusões não metálicas. Doutorado em Ciências e Engenharia de Materiais - Área: Metais - Universidade do Estado de Santa Catarina, Joinville, 2015. CDD620.16 – 23. ed.

RUBEN, Perez Mora. Study of the Fatigue Strength in the Gigacycle Regime of Metallic Alloys used in Aeronautics and Off-Shore Industries. Mechanics of materials [physics.class-ph]. Arts et Metiers ParisTech, 2010;

SAE International (Org.). SAE Fatigue Design Handbook. 3. ed. Warrendale, Pa: Ae-22, 1997;

SCOTT-Emuakpor, Onome et al. Bending Fatigue Life Comparison between DMLS and Cold-rolled Nickel Alloy 718. Air Force Research Laboratory. Dayton, Oh, p. 1-17. may 2014;

SORI, Marko et al. Fatigue Properties of Sintered DIN SINT-D30 Powder Metal Before and After Heat Treatment. Original Scientific Article UDK 621.762:539.43. 2014;

STRAFFELINI, G., Benedetti, M., Fontanari, V., Damage evolution in sinter - hardening powder metallurgy steels during tensile and fatigue loading, Materials and Design (2014) DOI: http://dx.doi.org/10.1016/j.matdes.2014.04.027;

TIWARI, Ambrish et al. Fatigue Analysis of Connecting Rod Using Finite Element Analysis to Explore Weight and Cost Reduction Opportunities for a Production of Forged Steel Connecting Rod. International Journal of Advanced Mechanical Engineering. ISSN 2250-3234 Volume 4, Number 7 (2014), pp. 782-802;

YAN, Yingjie; Nash, Guiru Liu; Nash, Philip. Effect of density and pore morphology on fatigue properties of sintered Ti–6Al–4V. International Journal Of Fatigue. Chicago, p. 81-91. jun. 2013.

A reciprocating compressor cranktrain design is highly dependent on the definition of its connecting rod. This component, usually sintered, is designed to convert rotational movement from electrical motor into linear movement of the piston, absorb mechanism components geometrical deviations and survive the compressor envelope operating loads.

Hence, this important component fatigue behavior must be evaluated through numerical simulations, experimental bench tests and field reliability evaluations in order to predict possible failure modes caused by different operating boundary conditions characterized by the combination of bending and compression.

This work aims to explore the sintered connecting rod mechanical properties at static and dynamic combination of tensile and compressive loads. Two S-N curves with compressive and zero mean stress levels are associated to generate a fatigue criteria and calculate the connecting rod safety factor, when running within the compressor operating envelope.

Advisor: Dr. Renato Barbieri

JOINVILLE, 2018